Loss of tumor suppressor WWOX enhances RAS activity in pancreatic cancer

Hussam Husanie[1], Muhannad Abu-Remaileh[1], Lina Abu-Tair[1], Hazem Safadi[1], Karine Atlan[2], Talia Golan[3], Rami I. Aqeilan[1,*]

[1]The Concern Foundation Laboratories, The Lautenberg Center for Immunology and Cancer Research, Department of Immunology and Cancer Research-IMRIC, Faculty of Medicine, The Hebrew University of Jerusalem, Jerusalem, Israel; [2]Department of Pathology, Hadassah Medical Center, Jerusalem, Israel; [3]Oncology Institute, Sheba Medical Center, Tel Aviv University, Israel.

* Corresponding author: ramiaq@mail.huji.ac.il

Keywords: Pancreatic cancer, WWOX, KRAS, ADM, MAPK, Stat3

Abstract

Pancreatic cancer is one of the most lethal cancers, due to late diagnoses and chemotherapy resistance. The tumor suppressor WWOX, spanning one of the most active common fragile sites in the human genome (FRA16D), is commonly altered in pancreatic cancer. However, the direct contribution of WWOX loss to pancreatic cancer development and progression is largely unknown. Here, we report that combined conditional deletion of *Wwox* and activation of *KRasG12D* in *Ptf1a-CreER*-expressing mice resulted in accelerated formation of precursor lesions and pancreatic carcinoma. In addition, these mice displayed enhanced MAPK and IL6/Jak/Stat3 signalling, combined with higher rates of macrophage infiltration and inflammation signature at sites of acinar to ductal metaplasia (ADM). Moreover, accumulated DNA double strand breaks were observed at ADM lesions. Finally, overexpression of WWOX in patient-derived xenografts led to reduction in KRAS MAPK activity and IL6/Jak/Stat3 signalling so diminishing their aggressiveness and *in vivo* tumor growth. Our data underscore the important role of WWOX in regulating RAS activity in pancreatic carcinogenesis.

Introduction

Pancreatic ductal adenocarcinoma (PDAC) is currently the fourth leading cause of cancer death in the modern world, with a five year survival rate of 9% of the patients (Siegel et al., 2019). Approximately, 15-20% of patients are eligible for surgical resection, the rest of the patients are inoperable or have advanced metastatic disease with minimal benefit to chemotherapy treatment (Ryan et al., 2014). PDAC is believed to develop in a gradual manner over time by accumulating mutations in a number of oncogenes and tumor suppressors (Hruban et al., 2000). Constant activation of oncogenic *KRAS* is one of the most frequent mutations found in human intraepithelial neoplasm (PanINs) and PDAC. For example, *Kras-G12D* was found to be a driver mutation in pancreatic mouse models needed for PanIN initiation, maintenance, and progression to PDAC(MP & CD, 2013). Excessive activation of *KRAS* has a wide range of outcomes in pancreatic acinar cells including cell death, metaplasia, fibrosis development resembling chronic pancreatitis, and PDAC development(Logsdon & Ji, 2009). Nonetheless, mutations in tumor suppressor genes are also necessary for the progression of PanINs to PDAC, such as mutations in *CDKN2A*, *TP53* and *SMAD4* (J et al., 2001)·(Moskaluk et al., 1997)·(Wilentz et al., 1998)·(Oncology, 2002). Despite identifying a plethora of driver genes in PDAC, its prognosis is still the worst among human cancers (Jemal et al., 2010)·(Siegel et al., 2015). Therefore, an in-depth understanding of the molecular mechanisms of additional genes associated with PDAC formation and identifying the molecular targets and pathways involved in this process would enhance our understanding of PDAC initiation and progression.

Recent studies using genome wide exome sequencing has identified new mutations and alterations contributing to PDAC development (Waddell et al., 2015). Among

these mutations, deletion of the WW domain-containing oxidoreductase (*WWOX*) gene, spanning one of the most active common fragile sites (CFSs) involved in cancer, has been identified (Bednarek et al., 2001). WWOX has been mapped to the unstable PDAC subtype, which is characterized by genomic instability and defects in DNA maintenance (Waddell et al., 2015). Importantly, PDAC tumors harbour reduction or, even loss of WWOX protein expression. In fact, all pancreatic cancer cell lines and 40% of primary tumors exhibit a significant reduction of WWOX protein expression (Kuroki et al., 2004). Interestingly, WWOX expression has been shown to gradually dwindle with progression of preneoplastic lesions (Nakayama et al., 2008). In addition to genomic aberrations, WWOX promoter hypermethylation is evident in some pancreatic cancer cell lines and primary pancreatic adenocarcinoma cases(Kuroki et al., 2004). Furthermore, restoration of WWOX protein expression into pancreatic cancer cell lines induces apoptosis and suppresses their tumorigenicity both *in vitro* and *in vivo* (Kuroki et al., 2004)·(Nakayama et al., 2008). More recently, it has been reported that PDAC patients harbouring a single nucleotide polymorphism at *WWOX rs11644322 G>A* display worse prognosis and reduced gemcitabine sensitivity (Schirmer et al., 2016). Despite these numerous studies, the direct role of WWOX in PDAC initiation and progression is largely unknown.

WWOX is an adaptor protein harbouring two WW domains that interact with proline-rich motifs of its partner protein, regulating its stability and functions(Tanna & Aqeilan, 2018). An impaired DNA damage response (DDR) is one of the hallmarks of pancreatic cancer (Macgregor-Das & Iacobuzio-Donahue, 2013). We recently demonstrated that WWOX enhances efficient DDR and DNA double strand break (DSB) repair through interacting and regulating the activity of ataxia telangiectasia-mutated (ATM), a major DNA damage checkpoint protein (Abu-Odeh et al., 2014),

which is also implicated in PDAC (Perkhofer et al., 2017). Regardless, WWOX's role in maintaining genome stability in pancreatic cancer is largely unknown.

In this study, we provide evidence that WWOX ablation leads to acceleration in acinar to ductal metaplasias (ADM), PanIN lesions and PDAC development. This enhancement takes place due to hyperactivation of Kras, resulting in inflammatory signalling and enhanced genome instability. Moreover, restoration of WWOX in patient-derived xenografts (PDXs) of PDAC suppressed tumor growth. Our findings indicate WWOX as a *bone fide* tumor suppressor in PDAC regulating *RAS* activity.

Results

Targeted WWOX deletion accelerates neoplastic lesion formation.

WWOX expression is reduced in PanINs (Nakayama et al., 2008) suggesting that WWOX may play a direct role in PanINs formation and progression. To determine WWOX's role in PDAC formation, we generated a newly genetically engineered mouse model harbouring *Wwox* deletion and *Kras* activation in pancreatic acinar cells and examined their phenotypes. To achieve this, we bred mice carrying a tamoxifen inducible Cre (CreER) that is controlled by the *Ptf1a* specific acinar promoter with a conditional tdTomato reporter (*Rosa26*-LSL-*tdTomato*) to generate *Ptf1a-CreER; Rosa26-LSL-tdTomato* wild type (WT) mice. These mice were then bred with conditional $Kras^{G12D}$ knock-in mice to generate *Kras+/LSL-G12D; Ptf1a-CreER; Rosa26-LSL- tdTomato*, hereafter referred to as KC mice. *Wwox-floxed* mice (*Wwoxf/+* or *Wwoxf/f*) (SK et al., 2013) were next bred with the KC mice to generate the KWC mice (*Wwox(f/f* or *+/f);Kras+/LSL-G12D; Ptf1a-CreER; Rosa26-LSL-*

tdTomato) and WC (*Wwox(f/f)(+/f); Ptf1a-CreER; Rosa26-LSL- tdTomato)* mice (Fig. 1a). The models were validated by genotyping with specific primers suitable for each allele (*Cre*, *Wwox*, and *Ras* respectively) (Fig. S1a), by detecting tomato colour by brightfield imaging (Fig. S1b), immunoblot analysis (Fig. S1c), by immunostaining for WWOX, tdTomato and/or amylase (Fig. S1e-g). Successful tamoxifen activation of Cre was assessed in four-week old mice by validation of tomato expression using immunofluorescence and specific acinar ablation of WWOX and pERK using immunohistochemical staining (Fig. 1b).

We next monitored and carefully analysed the pancreas in adult WC, KC and KWC mice at different time points. H&E stain of pancreata of these mice revealed enhanced ADMs and PanINs formation in KWC mice compared to KC mice; lesions appeared as early as one month in the KWC mice (Fig. 1c). No phenotypes were identified in pancreata of WC mice suggesting that *Wwox* deletion alone is not sufficient for ADM and PanIN lesions (Fig. S1d). Quantification of ADM and low grade PainIN lesions at one month post-tamoxifen injection revealed a significantly increased number in KWC mice compared to KC mice (Fig.1d). No differences were observed between KWC mice harbouring *Wwoxf/+* or *Wwoxf/f alleles.* Moreover, tdTomato sorted cells from mice two months post-tamoxifen injection revealed an induction in *Runx1*, *Onecut2*, and *Foxq1*, genes shown to be associated with ADM reprogramming (Fig. S1f) (Schlesinger et al., 2020). In addition, there was an increased rate of proliferation at these lesions as assessed by Ki-67 (Fig. 1h, i). Remarkably, some lesions progressed with time to form PDAC tumors in the KWC but not in the KC mice (Fig. 1c). These findings suggest that WWOX loss accelerates Kras-mediated ADM and PanIN lesions and promotes progression to PDAC formation.

WWOX **deletion accelerates PDAC formation.**

Our previous observations prompted us to further follow aging KC and KWC mice to monitor PDAC formation. To this end, mice were injected with tamoxifen at the age of one month, then followed for another eight months. Interestingly, 16 out of 64 *Wwoxf/+* or *Wwoxf/f* KWC mice formed tumors between the ages 4-8 months while none of the KC mice (n=14) did in this time range (Fig. 2a). Histological characterization of KWC tumors revealed aggressive and highly proliferative tumors, with tomato expression confirming acinar cells as the origin of the tumors (Fig. 2b). Intriguingly, *Wwoxf/+* KWC mice developed pancreatic tumors at the same rate as *Wwoxf/f* KWC mice. We therefore stained for WWOX protein expression in tumors that developed in *Wwoxf/+* KWC mice and found loss of WWOX staining at the tumor site, suggesting loss of *Wwox* heterozygosity (Fig. 2c). The tumors formed were rich in spindle-shaped cell morphology, positive for pancytokeratin marker and negative for amylase staining, indicating mesenchymal identity (Fig. 2c). In addition, the tumors were highly positive for pERK, pStat3, and EMT markers confirming their aggressiveness (Fig. 2c, e). Liver, lung, and spleen metastases were found in 3 out of the 16 KWC tumor-bearing mice. These metastatic lesions were positive for tomato reporter, negative for WWOX IHC and highly expressed pancytokeratin, pERK, and pStat3 suggesting they were of PDAC origin (Fig. 2d). To exclude the possibility of *Ptf1a* promoter leakage to distant sites such as liver and lung, we stained for tomato in WT mice expressing tomato post-tamoxifen injection. Liver and lung tissues (n=3) were negative for tomato whereas pancreatic tissues were positive, suggesting that the origin of the metastases is the primary tumors, and they were not due to leakage of Ptf1a expression (Fig. S2b). Altogether, our findings indicate acceleration of Kras-mediated PDAC carcinoma formation upon deletion of *Wwox*.

WWOX accelerates formation of lesions by regulating Kras signalling.

To shed light on the molecular mechanism of WWOX in accelerating lesion formation, total RNA from 3 WT mice, 3 KC mice and 5 KWC mice (3 *Wwoxf/+* and 2 *Wwoxf/f*) at two months post-tamoxifen injection was extracted from tomato-sorted acinar cells and RNA sequencing (RNA-seq) was performed. Bioinformatic analysis revealed 1381 genes that were differentially expressed in KWC and KC mice (Supplementary Table 1). Principle component analysis (PCA) showed a clear separation between all groups (WT, KC, and KWC mice). The differentially expressed genes were enriched for pathways known to be implicated in WWOX signaling such as hypoxia (Muhannad Abu-Remaileh et al., 2019),(Muhannad Abu-Remaileh et al., 2018),(M. Abu-Remaileh & Aqeilan, 2014) and DDR (RI et al., 2014) and other emerging ones including *Il6/Jak/Stat3*, *Kras* signalling and inflammatory response (Fig. 3b). Since the prominent outcome of *Wwox* deletion was an increase in the number of early precursor lesions, mainly ADM (Fig 1), we hypothesized that the enrichment in the differentially expressed genes at 2-months post-tamoxifen mainly stems from changes in early precursor lesions. To validate enrichment in the Kras signalling, we performed pERK staining in KC and KWC pancreata at one-month post-tamoxifen injection. Strikingly, Kras signalling was clearly enhanced in KWC compared to KC mice at this early time point (Fig. 3c, d).

One of the main pathways activated by oncogenic Ras in early precursor lesions is the *Il6/Jak/Stat3* signaling pathway (Gruber et al., 2016). Staining for pStat3 (Y705) revealed elevated expression of pStat3 in ADM lesions in KWC mice compared to KC mice. In addition, RNA-seq data revealed downregulation of Socs3, a negative

regulator of Stat3, in KWC mice relative to KC mice (Fig. S3a). A major outcome of Stat3 activation is inflammation, by promoting the expression of crucial inflammatory genes including *Il6*, *Il10*, *Il11*, *Il17*, *Il23*, *Cxcl12*, and *Cox-2* (Yu et al., 2009),(Sikka et al., 2014). We therefore tested for COX-2 protein expression as an inflammatory downstream effector of Stat3 and found an increased number of cells positively stained for COX2 in the ADM lesions of KWC pancreata (Fig. 3g, h, c). Furthermore, RNA-seq data demonstrated an induction of *Cox2* and *Il6* transcripts in KWC mice relative to KC mice (Fig. S3c, d). As macrophages can activate *Stat3* signalling to promote *Il6* secretion and hence trans-signal to activate Stat3 in pancreatic epithelial cells (Lesina et al., 2011), we performed IHC staining with F4/80, a surrogate marker of macrophages, and confirmed enrichment in the number of macrophages in KWC mice compared to KC mice (Fig. 3i, j). Taking these findings together, we conclude that WWOX ablation contributes to lesion progression through regulating hyperactivation of Kras signalling, which in turn activates the Il6/Jak/Stat3 inflammatory pathway.

WWOX ablation enhances DSBs and genome instability.

Oncogene activation such as *KrasG12D* enhances genome instability by inducing replication stress(Kotsantis et al., 2018). Moreover, perturbation in genes responsible for the DDR such as WWOX accelerates accumulation of DSBs and genome instability (Abu-Odeh et al., 2015),(Abu-Odeh et al., 2014). Therefore, we hypothesised that WWOX ablation in our model could contribute to lesion progression through accumulation of DSBs. To test our hypothesis, pancreata from mice of the different genotypes one and two months post-tamoxifen injection were stained for γH2AX and

53BP1, surrogate markers of DSBs. As expected, WT mice had low foci count of DSBs with an average of ~0.4% and 0.6% foci/nuclei for γH2AX and 53BP1 respectively, at one and two-months post-tamoxifen injection (Fig. 4a-d, Fig. S4a-d). On the other hand, a clear accumulation of DNA damage in ADM lesions of KC and even more in KWC mice was observed (Fig. 4a-d, Fig. S4a-d). These results suggest that WWOX ablation is critical to ADM lesions and that its loss promotes enhanced DNA damage.

KRAS activation induces WWOX expression.

The preceding observations suggest that WWOX loss enhances KRAS signalling, but does KRAS activation modulate WWOX levels or function? To address this, we examined WWOX protein expression in pancreata of KC mice. Upon Kras activation in KC mice, cytoplasmic expression of WWOX was gradually lost with lesion progression (Fig. 5a), as revealed by IHC staining. These findings were consistent with a previous observation of gradual loss of WWOX expression in human pancreatic tumor samples(Nakayama et al., 2008). As WWOX's critical function is linked to early ADM lesions (Fig. 1, 3 & 4), we determined WWOX expression upon Kras activation in early lesions. To this end, we stained for WWOX in pancreata of WT and KC mice at 1, 2, 4, and 8 weeks post-tamoxifen injection. Strikingly, WWOX protein expression was increased in acinar cells upon Kras activation compared to WT mice (Fig. 5b, c). In addition, qRT-PCR analysis revealed an upregulation of *Wwox* RNA expression in KC mice from sorted tomato acinar cells at 8 weeks post-tamoxifen injection compared to acinar cells sorted from WT mice (Fig. 5d).

To further confirm the effect of Kras activation on WWOX levels using a different system, we utilised the 266-6-Tet on/off KrasG12D murine acinar cells. Treatment of

these cells with doxycycline for 6, 24, and 48 h increased levels of pErk, as revealed by western blot (Fig. 5e). Importantly, *Kras* activity was accompanied by induction of *Wwox* protein levels and upregulation of mRNA expression (Fig. 5e, g). We conclude that Kras activation initially results in induction of WWOX levels followed by its downregulation and likely progression to advanced lesions.

Overexpression of WWOX in pancreatic cancer patient-derived xenografts (PDXs) suppresses their tumorigenicity.

To further validate the effects of WWOX using a human system, we assessed its expression in five PDX lines derived from advanced tumors (50, 92, 114, 134, and 139). As seen in Fig 6a, WWOX expression was found to be reduced in three out of the five PDXs [92, 134 and 139]. Interestingly, p-ERK amount was prominent in PDX139. We next transduced all PDXs using a lenti-WWOX vector or empty vector (EV) and generated stable lines, which were validated by immunoblotting (Fig 6a, b). Interestingly, WWOX restoration in PDX92, 134, and 139, harbouring low WWOX expression, successfully reduced pERK and pSTAT3 expression. To validate the biological effect of WWOX restoration *in vitro*, we performed colony formation assays for PDX50, 92, 134, and 139 (WT, EV, and WWOX overexpression (OE)). We found that WWOX restoration in PDX92, 134, 139, successfully suppressed colony formation (Fig. 6c, S6a,d). In contrast, WWOX overexpression had no effect on PDX50 and PDX114 (Fig. S6d). Next, we intraperitonially injected PDX139 EV and OE into NOD/SCID mice to reveal whether WWOX restoration has any effect on *in vivo* tumor formation. Indeed, PDX139 with WWOX overexpression resulted in smaller and lighter tumors compared to PDX139, and PDX139 EV (Fig. 6d, e). Staining tumors of

PDX139, EV and OE, revealed higher expression of pERK and pStat3 in PDX139, and PDX139 EV compared to PDX139 WWOX OE, further confirming WWOX's function in Kras and Stat3 signalling (Fig. 6F). Finally, restoration of WWOX in PDX139 successfully reduced the number of γH2AX foci/nuclei to 29% compared to 74.7%, and 71.3%, respectively in PDX139 and PDX139 EV (Fig S6b, c). These findings further imply an important role of WWOX in pancreatic tumor development.

Discussion

Pancreatic cancer patients have the lowest survival rates among cancer patients, mainly due to late diagnoses and limited benefit of standard of care treatments (Jemal et al., 2010),(Siegel et al., 2015).Therefore, understanding the molecular changes and pathways contributing to PDAC is critical to improve survival rates. In previous studies, WWOX has been reported to be lost in pancreatic cancer cell lines, either by deletion or promoter hypermethylation (Kuroki et al., 2004),(R et al., 2010),(A & RI, 2014). In addition, restoration of WWOX expression to these cell lines supresses cell growth both *in vitro* and *in vivo* and induces apoptosis (N. S et al., 2008). In our current study, we found that somatic WWOX loss combined with oncogenic activation (*RasG12D*) in the Ptf1a mouse model result in accelerated formation of pancreatic tumors. Dissection of the plausible mechanism uncovered a functional crosstalk between WWOX and RAS signalling. These results further underscore the tumor suppressor function of WWOX in pancreatic carcinogenesis.

Prior studies have shown gradual loss of WWOX expression with progression of preneoplastic lesions in pancreatic cancer (N. S et al., 2008). Here, we report for the first-time successful recapitulation of this phenomenon in a mouse model harbouring

Ras activation, one of the major hallmarks of pancreatic cancer. Our findings reveal that WWOX acts as a barrier that when breached, tumors can progress, as evident from increased proliferation and appearance of malignant and metastatic tumors in KWC mice. This barrier seems to be critical in early ADM lesions, as KC mice exhibited increased WWOX levels. Previous observation has indeed shown that WWOX levels are increased upon DNA damage insult (Abu-Odeh et al., 2014),(Abu-Odeh et al., 2015). Combined targeted deletion of *Wwox* and Kras activation enables ADM reprogramming, an important step in PDAC development (Wang et al., 2019). Recently, a number of specific genes have been proposed to be associated with the ADM process in pancreatic carcinogenesis including *Onecut2* and *Foxq1* (Schlesinger et al., 2020). Interestingly, these genes were upregulated in tomato-positive cells isolated from KWC mice, as revealed by RNA-seq data.

Little is known about WWOX's contribution to pancreatic cancer at the molecular level. One study suggested WWOX to suppress pancreatic cancer through upregulating SMAD4 signalling in Panc1 cells(N. S et al., 2008). Using our model of pancreatic cancer, we found that WWOX loss results in activation of several known pathways implicated in PDAC formation, some of which have been previously linked with WWOX function such as hypoxia (Muhannad Abu-Remaileh et al., 2019),(Muhannad Abu-Remaileh et al., 2018),(M. Abu-Remaileh & Aqeilan, 2014) and DDR (Abu-Odeh et al., 2015) signalling. This included enhanced Ras signalling and inflammation, activation of the p53 pathway and DNA damage signalling. Intriguingly, all these pathways could be mediated by enhanced MAPK signalling of RAS resulting in acute and chronic inflammation(Hamarsheh et al., 2020). Patients with history of familial pancreatitis, involving germline mutation in genes such as *PRSS1* and *SPINK1*, have 69-fold higher probability to develop PDAC(Kitajima et al., 2016). RAS can induce inflammation

through enhancing secretion of cytokines, which will induce infiltration of myeloid cells and particularly macrophages that secret IL-6 to activate Stat3 inflammatory signature(Lesina et al., 2011). The effect of WWOX deletion on enhanced MAPK signalling recapitulates these events in KWC mice leading to higher infiltration of macrophages, which is accompanied by an increased inflammatory response, manifested by increased *Cox2* and *Il6/Stat3* signalling. As WWOX loss has been shown to enhance IL6/Stat3 signalling in triple-negative breast cancer (TNBC) cells (Chang et al., 2018), we assume that WWOX has an important function in regulating the inflammatory stress response.

Characterization of our new mouse model also revealed an *in vivo* function of WWOX in regulating DSB repair and genome stability. Continuous activation of oncogenes, such as KRAS, does not only regulate cell cycle entry but can also induce replication stress through stalling and collapse of the replication fork, leading to DSBs formation at preneoplastic and carcinoma sites (Gorgoulis et al., 2005),(Bartkova et al., 2006),(Halazonetis et al., 2008). Continuous accumulation of DSBs, present in an enormous number of tumors, may contribute to genome instability (Halazonetis et al., 2008). Upon replication stress, CFSs are expressed in metaphase chromosomes (L. S & X, 2020). Since WWOX spans one of the most active fragile sites FRA16D (Bednarek et al., 2001), it is possible that WWOX can be lost. Paradoxically, it has been shown that products of CFSs can play a direct role in the DDR (RI et al., 2014),(CE et al., 2014),(AG et al., 2014). In addition, several studies have shown upregulation of WWOX expression *in vitro* upon DNA damage (Abu-Odeh et al., 2015),(Abu-Odeh et al., 2014),(Abdeen et al., 2018). Furthermore, WWOX physically interacts with DNA damage checkpoint proteins such as ATM and BRCA1 to regulate DNA repair (Abu-Odeh et al., 2014),(Abu-Odeh et al., 2015),(MS et al., 2017),(Schrock

et al., 2017). Our current *in vivo* data indeed reveal that WWOX levels are induced upon RAS activation, likely as a stress response to oncogene activation. Importantly, deletion of WWOX is associated with accumulation of DSBs at sites of preneoplastic lesions mainly at ADM sites. Increased WWOX expression was also recapitulated in an *in vitro* system (266-6 cells) upon activation of RAS and in human PDX lines. These findings imply that WWOX is involved in regulating genome stability in PDAC formation.

We suggest a model (Fig. 7) in which continuous RAS activation, an early event in PDAC, will lead to an unstable genome. As a result, WWOX expression, among that of other proteins, is induced to act as a barrier to effectively activate the DNA damage protein checkpoints and to repair the damage. Gradual loss of WWOX, possibly due to its genomic localization at FRA16D, could facilitate formation of preneoplastic lesions as indicated in our results. Once the WWOX barrier is lost in preneoplastic lesions, additional DSBs accumulate enhancing the oncogenic activity of RAS and its inflammatory signature. In essence, our data leads us to propose that deletion of WWOX synergizes with RAS activation to accelerate formation of the preneoplastic lesions, tumor development and metastasis. These findings further underscore the significance of tumor suppressor genes spanning common fragile sites and their active roles in carcinogenesis.

Materials and methods:

Mice

Mice purchased from the Jackson Laboratory (stock #00790875(L et al., 2010), stock #01937876(D et al., 2012), and stock #00817977(EL et al., 2001)) were crossed to generate the following: wild type mice (*Ptf1a-CreER; Rosa26-LSL- tdTomato)*, KC mice (*Kras+/LSL-G12D; Ptf1a-CreER; Rosa26-LSL- tdTomato)*, and *Wwox-floxed (Wwoxf/f)* C57BL6/J; 129sv mixed genetic background mice(SK et al., 2013) were crossed with KC mice to generate KWC mice: (*Wwox(f/f)/(+/f);Kras+/LSL-G12D; Ptf1a-CreER; Rosa26-LSL- tdTomato)*. Tamoxifen, dissolved in corn oil (Sigma: C8267), was subcutaneously injected to mice aged four weeks; two doses of 400 mg/kg were injected 48 h apart. All experiments involving mice were approved by The Hebrew University Institutional Animal Care and Use Committee [#MD-18-15468-5].

PDX injection in mice

1×10^6 cells of PDX139, EV, and WWOX OE were suspended in DMEM medium and injected intraperitoneally (IP) into 6-8 weeks old NOD/SCID mice, to study the ability of these cells to form tumors. Tumor volume and weight were measured at time of collection, 35-days after IP-injection. Mice were euthanized and primary tumors were collected for H&E and IHC staining.

Cell culture and plasmids

266-6 cells were obtained from Dr. Oren Parnas's lab (Hebrew University of Jerusalem) and grown in DMEM (Gibco) supplemented with 10% FBS, 1% glutamine, 1% penicillin/streptomycin, and 1% sodium-pyruvate (Biological Industries). Prior to culturing, plates were coated with 0.1% gelatin Type A (Sigma: G2500) followed by

refrigerating the plates for 10-15 min, removal of gelatin, and then rinsing the plates gently with medium before culturing the cells. For producing 266-6 KRAS cells, 266-6 CAS9 cells were infected with FUW-TetO-KRASG12D-BleoR virus, and cells were selected with 5 ug/ml zeocin (Invivogen, San Diego, CA) for 10 days. These cells were subsequently transduced with rtTA-tdTomato virus and were sorted for tdTomato positive cells by FACSAriaII. For producing WWOX overexpression in PDX cell lines, cells were infected with lentiviral vector containing the wild type WWOX and selected with 2 mg/mL G418 (Gibco: 11811031). For inducing KRAS expression in 266-6 cells 2 µg/mL doxycycline (Tamar Laboratory Supplies) was added to medium at different time points. PDX cells(Golan et al., 2021) were cultured in DMEM (Gibco) supplemented with 10% FBS, 1% glutamine and 1% penicillin/streptomycin. All cells were grown in 37°C with 5% CO_2.

Colony formation assay

500 cells from each PDX cell line were plated in triplicates in 60 mm^2 plates for 10-14 days; cells then were fixed by 70% ethanol, stained with Giemsa, and counted.

Histology and Immunohistochemistry

Tissues were fixed with 4% formalin, followed by paraffin embedding and sectioning then stained with haematoxylin and eosin for histology. For immunohistochemistry (IHC), paraffin embedded tissues were deparaffinized followed by antigen retrieval with 25 mM citrate buffer pH 6 in a pressure cooker. Then the sections were left to cool for 25 min, followed by blocking of the endogenous peroxidase with 3% H_2O_2 for 15 min. To reduce non-specific binding of the primary antibody, tissues were blocked with blocking solution (CAS Block) (Invitrogen) followed by incubation of the primary antibody overnight at 4°C. Sections were washed with TBST followed by incubation of

the secondary anti-rabbit or anti-mouse immunoglobin antibody for 30 min. The reaction was then performed using a DAB peroxidase kit (Vector laboratories: SK-4100), followed by haematoxylin stain for 40 s as a counter stain. IHC stains were manually counted, and for each slide at least five pictures were taken, and the average was calculated for each slide.

Immunofluorescence

Paraffin embedded sections were used to perform immunofluorescence (IF) staining. Deparaffinization and antigen retrieval was performed as described previously for IHC. Sections were then blocked for one hour using a blocking solution containing 5% normal goat serum, 0.5% BSA, and 0.1% Triton X-100 in PBS (Biological Industries). Sections were then incubated with primary antibody at 4°C overnight. On the following day, sections were washed three times with PBS and then incubated with the secondary antibody and Hoechst solution, diluted in the blocking buffer, for one hour. Slides were washed three times with PBS, dried, and mounted with coverslips using fluorescence mounting medium (Dako: S3023). IF stains were manually counted, and for each slide at least three pictures were taken, and the average was calculated for each slide.

Isolation of acinar cells and sorting

Mice were euthanized by CO_2, followed by pancreas removal and washing with cold HBSS (Biological Industries). The pancreas was then cut into 1-2 mm pieces in cold HBSS and centrifuged at 600 rpm for 5 min at 4℃. For the first dissociation step, the pieces were resuspended with 0.05% trypsin-EDTA (solution C, Biological Industries) at final concentration of 0.02% for 15 min shaking at 37℃, followed by washing with

10% FBS/DMEM to stop the reaction. Then cells were centrifuged at 600 rpm followed by washing with 4% bovine serum albumin (BSA) (Mpbio) prepared in HBSS containing 0.1 mg/ml DNase I (Sigma). For the second dissociation step, cells were resuspended with 4% BSA containing 0.1 mg/ml DNase I, and 10 mg/ml collagenase P (Sigma) at final concentration of 1 mg/ml of collagenase P. Cells were incubated for 20-30 min at 37℃ with shaking, and they were pipetted up and down 10 times every 5 minutes of the incubation. Cells were then passed through a 100 μm cell strainer (Corning) and washed with 4% BSA prepared in HBSS containing 0.1 mg/ml DNase I. The samples were then treated with red blood cell lysing buffer (Sigma Aldrich) and passed through a 40 μm cell strainer (Corning) and submitted for tdTomato sorting using BD FACSAria III or Sony SH800.

RNA extraction, cDNA preparation and qRT-PCR

TRI reagent (Biolab) was used as described by the manufacturer to prepare total RNA. To prepare cDNA, 1 ug of RNA was used using the QScript cDNA synthesis kit (Quantabio). SYBR Green PCR Master Mix (Applied Biosystems) was used to perform the qRT-PCR. All measurements were done in triplicates and normalized to the levels of *Ubc* or *Hprt* genes.

Immunoblotting

Total protein was lysed by using lysis buffer containing 50 mM Tris (pH7.5), 150 mM NaCl, 10% glycerol, 0.5% Nonidet P-40 (NP-40), with addition of protease and phosphatase inhibitors (1:100). Lysates were run on SDS/PAGE under standard conditions. Antibodies used were polyclonal WWOX, monoclonal GAPDH (Calbiochem), monoclonal ERK (Cell Signaling), monoclonal pERK (Cell Signaling), monoclonal STAT3 (Cell Signaling), monoclonal pSTAT3 (Abcam).

RNA-sequencing

3 WT, 3 KC, and 5 KWC mice were euthanized by CO_2, pancreata were disassociated and tdTomato acinar cells were sorted using BD FACSAria III. Preparation of the libraries and sequencing were performed by the Genomic Applications Laboratory in the Hebrew University's Core Research Facility using standard protocol. RNA quality was checked using tape-station (Agilent Technologies), followed by poly-A clean-up and cDNA preparation. For preparing the cDNA, 1 μg of RNA from each sample was processed using KAPA Stranded mRNA-Seq Kit with mRNA Capture Beads (Kapa Biosystems). Then sequencing was performed using NextSeq 500 (Illumina). For library quality control, measures were applied to raw FASTQ files, trimming low quality bases (Q>20), residual adapters and filtering out short reads (L>20). These measures were performed with the Trim-Galore (v0.4.1) wrapper tool. File assessment before and after quality control was performed with FastQC (v0.11.5). Mapping the mouse transcriptome was done using Salmon v0.13.1. Differential gene expression for the 11 samples was explored by R package (v1.16.1) and analysed with DESeq2 (v1.28.1).

Acknowledgements: We are grateful to all members of the Aqeilan lab for fruitful discussion and suggestions. We thank Jonathan Monin for bioinformatics assistance.

Contributors: HH and RIA designed the study and wrote the manuscript, HH, MA and LA-T conducted the experiments, KA conducted pathological analyses, HS performed bioinformatic analysis.

Funding: This study was supported by donations from The Alex U Soyka Pancreatic Cancer Research Project (RIA, HH) and grants from the European Research Council

(ERC) [No. 682118] (RIA) and the Israel Cancer Research Fund (ICRF) postdoctoral fellowship (LA-T).

Competing interests: none.

Figure Legends

Figure 1. *WWOX* deletion synergies with *K-ras* activation by accelerating neoplastic lesions formation. (A) Illustration of KWC mice generation (*Wwox(f/f)/(+/f)(W);Kras+/LSL-G12D(K); Ptf1a-CreER(C); Rosa26LSL- tdTomato.* (B) Validation of the KWC model by immunofluorescence for tdTomato, WWOX, and pERK IHC stain respectively (magnification, ×4, ×40, and ×40 respectively). (C) Representative haematoxylin and eosin (H&E) stain for the pancreas at 1,2,3,4,5, and 6 months respectively (magnification, ×4). (D) Quantification of lesions for KC mice, n=4, and KWC mice, n=9, 4 weeks post tamoxifen injection. (E) Representative Alican blue stain, 4 weeks post tamoxifen injection (magnification, ×40). (F) Representative Ck19 stain, 4 weeks post tamoxifen injection (magnification, ×20). (Magnification, ×20). (G) Quantification of Ck-19 stain in figure (F). (H) Representative Ki-67 stain, 4 weeks post tamoxifen injection (magnification, ×20). (I) Quantification of Ck-19 stain in figure (H). NS>0.05, ***P*<0.001, ****P*<0.0001. Two tail unpaired t test with Welch`s correction. Quantification graphs represent the means ± SD.

Figure 2. Characterisation of pancreatic tumors in KWC mice. (A) 0 out of 14 KC mice compared to 16 out of 64 KWC mice formed tumors between 4-8 months (only KWC mice are presented on the graph). (B) Upper panel, representative H&E and tomato staining for a KWC normal site (magnification ×10 and ×40, respectively). Lower panel, representative H&E and tomato staining for a KWC carcinoma site (magnification ×10 and ×40, respectively). (C) Upper panel, representative WWOX, pancytokeratin, pERK, pStat3, and amylase of KWC normal site (magnification ×10). Lower panel, representative WWOX, pancytokeratin, pERK, pStat3, and amylase of

KWC carcinoma site (magnification ×10). (D) Upper panel, representative H&E and tomato stain for metastasis site (magnification ×10 and ×40, respectively). Lower panel, representative WWOX, pancytokeratin, pERK, pStat3, and amylase of KWC metastatic site (magnification ×10). (E) Representative tomato, E-cadherin, and vimentin stain of KWC carcinoma site (magnification ×40).

Figure 3. Hyperactivation of K-ras signalling upon WWOX ablation. (A) A principal component analysis (PCA) of pancreas tissue from WT mice (n=3), KC mice (n=3), and KWC mice (n=5) 8 weeks post tamoxifen injection. (B) Molecular Signatures Database analysis (MSigDB) of differentiated genes comparing KWC and KC mice. (C) Representative pERK stain in KC and KWC mice, respectively (magnification ×10). (D) Quantification of pERk for KC mice n=4, and KWC mice n=9 at 4 weeks. (E) Representative pStat3 stain in KC and KWC mice respectively (magnification ×20). (F) Quantification of pStat3 for KC mice n=4, and KWC mice n=9 at 4 weeks. (G) Representative Cox2 stain in KC and KWC mice respectively (magnification ×20). (H) Quantification of Cox2 for KC mice n=4, and KWC mice n=9 at 4 weeks. (I) Representative F4/80 stain in KC and KWC mice, respectively (magnificatio, ×20). (J) Quantification of F4/80 for KC mice n=4, and KWC mice n=9 at 4 weeks. *P<0.05, **P<0.001. Two tail unpaired t test. Quantification graphs represent the means ± SD.

Figure 4. Accumulation of double strand breaks upon deletion of WWOX. (A) Representative γH2AX stain at ADM site of WT (n=3), KC (n=4), and KWC mice (n=4) respectively, 4 weeks post tamoxifen injection (magnification ×60). (B) Quantification of *γH2AX* stain in A. (C) Representative γH2AX stain at ADM site of WT (n=3), KC

(n=3), and KWC mice (n=4) respectively, 8 weeks post tamoxifen injection (magnification ×60). (D) Quantification of γH2AX stain in C. NS>0.05, **P*<0.05, ****P*<0.0001, by two tail unpaired t test. Quantification graphs represent the means ± SD.

Figure 5. Induction of WWOX expression upon K-ras activation. (A) Representative WWOX stain at acinar and PanIN sites (magnification ×40). (B) Representative WWOX stain for WT, and KC mice after 1,2,4, and 8 weeks post tamoxifen injection respectively. (C) Representative Western blot of whole pancreas for WT, KC, and KWC mice one month post tamoxifen injection (D) RT-PCR of sorted acinar cells from WT, KC, and KWC mice 8 weeks post tamoxifen injection. (E) Western blot of WWOX, ERK, and pERK for 266-6, and 266-6 with doxycycline activation at 6, 24, and 48 h (F) RT-PCR of WWOX for 266-6, and 266-6 with doxycycline activation at 6, 24, and 48 h. (G) RT-PCR of K-ras for 266-6, and 266-6 with doxycycline activation at 6, 24, and 48 h. **P*<0.05, ***P*<0.001, ****P*<0.0001, by unpaired t test. Quantification graphs represent the means ± SD.

Figure 6: Restoration of WWOX to patient derived xenografts (PDX) with low WWOX expression reduce PDX aggressiveness. (A) Western blot of GAPDH, Stat3, pStat3, pERK, and WWOX of five PDXs, and their WWOX overexpression. (B) Western blot quantification of WWOX, pERK, and pStat3, respectively. (C) Quantification of colony formation for PDX 139, PDX 139 EV, and PDX 139 WWOX O.E. (D) Average tumor size of PDX 139 (n=4), PDX 139 EV (n=5), and PDX 139 WWOX O.E (n=6). (E) Average tumor weight of PDX 139 (n=4), PDX 139 EV (n=5), and PDX 139 WWOX O.E (n=6). (F) Representative H&E, WWOX, pERK, and pStat3

stain respectively for PDX 139, PDX 139 EV, PDX 139 WWOX OE (magnification ×10). NS>0.05, *P<0.05, ***P<0. 0001 by two tail unpaired t test. Quantification graphs represent the means ± SD.

Figure 7. Schematic model deciphering the role of WWOX in PDAC formation and progression. Upper panel - oncogenic activation of K-ras enhancing replication stress and DNA damage leading to upregulation of tumor suppressor WWOX to activate the DNA damage response machinery (DDR) and eliminate the damage. Continuous activation of K-ras will eventually cause the escape of some DNA damaged cells, which will secret proinflammatory factors in order to recruit the immune system (mainly macrophages) and in return they will signal back IL6 to these cells leading to the activation of pSTAT3 and eventually the formation of ADM lesions. Lower panel- Deletion of WWOX under oncogenic activation of K-ras will accelerate the accumulation of DNA damaged cells and the formation of ADM lesions.

References

A, G., & RI, A. (2014). WW domain-containing oxidoreductase's role in myriad cancers: clinical significance and future implications. *Experimental Biology and Medicine (Maywood, N.J.)*, *239*(3), 253–263. https://doi.org/10.1177/1535370213519213

Abdeen, S. K., Ben-David, U., Shweiki, A., Maly, B., & Aqeilan, R. I. (2018). Somatic loss of WWOX is associated with TP53 perturbation in basal-like breast cancer. *Cell Death & Disease 2018 9:8*, *9*(8), 1–13. https://doi.org/10.1038/s41419-018-0896-z

Abu-Odeh, M., Hereema, N. A., Aqeilan, R. I., Abu-Odeh, M., Hereema, N. A., & Aqeilan, R. I. (2015). WWOX modulates the ATR-mediated DNA damage checkpoint response. *Oncotarget*, *7*(4), 4344–4355. https://doi.org/10.18632/ONCOTARGET.6571

Abu-Odeh, M., Salah, Z., Herbel, C., Hofmann, T. G., & Aqeilan, R. I. (2014). WWOX, the common fragile site FRA16D gene product, regulates ATM activation and the DNA damage response. *Proceedings of the National Academy of Sciences*, *111*(44), E4716–E4725. https://doi.org/10.1073/PNAS.1409252111

Abu-Remaileh, M., & Aqeilan, R. I. (2014). Tumor suppressor WWOX regulates glucose metabolism via HIF1α modulation. *Cell Death and Differentiation*, *21*(11), 1805–1814. https://doi.org/10.1038/CDD.2014.95

Abu-Remaileh, Muhannad, Abu-Remaileh, M., Akkawi, R., Knani, I., Udi, S., Pacold, M. E., Tam, J., & Aqeilan, R. I. (2019). WWOX somatic ablation in skeletal

muscles alters glucose metabolism. *Molecular Metabolism*, *22*, 132–140. https://doi.org/10.1016/J.MOLMET.2019.01.010

Abu-Remaileh, Muhannad, Khalaileh, A., Pikarsky, E., & Aqeilan, R. I. (2018). WWOX controls hepatic HIF1α to suppress hepatocyte proliferation and neoplasia. *Cell Death & Disease*, *9*(5). https://doi.org/10.1038/S41419-018-0510-4

AG, G., P, T., A, K., I, M., P, T., & VG, G. (2014). Are common fragile sites merely structural domains or highly organized "functional" units susceptible to oncogenic stress? *Cellular and Molecular Life Sciences : CMLS*, *71*(23), 4519–4544. https://doi.org/10.1007/S00018-014-1717-X

Bartkova, J., Rezaei, N., Liontos, M., Karakaidos, P., Kletsas, D., Issaeva, N., Vassiliou, L. V. F., Kolettas, E., Niforou, K., Zoumpourlis, V. C., Takaoka, M., Nakagawa, H., Tort, F., Fugger, K., Johansson, F., Sehested, M., Andersen, C. L., Dyrskjot, L., Ørntoft, T., … Gorgoulis, V. G. (2006). Oncogene-induced senescence is part of the tumorigenesis barrier imposed by DNA damage checkpoints. *Nature*, *444*(7119), 633–637. https://doi.org/10.1038/NATURE05268

Bednarek, A. K., Keck-Waggoner, C. L., Daniel, R. L., Laflin, K. J., Bergsagel, P. L., Kiguchi, K., Brenner, A. J., & Aldaz, C. M. (2001). WWOX, the FRA16D gene, behaves as a suppressor of tumor growth. *Cancer Research*, *61*(22), 8068–8073.

CE, W., JC, S., SA, H., & K, H. (2014). The FHIT gene product: tumor suppressor and genome "caretaker." *Cellular and Molecular Life Sciences : CMLS*, *71*(23),

4577–4587. https://doi.org/10.1007/S00018-014-1722-0

Chang, R., Song, L., Xu, Y., Wu, Y., Dai, C., Wang, X., Sun, X., Hou, Y., Li, W., Zhan, X., & Zhan, L. (2018). Loss of Wwox drives metastasis in triple-negative breast cancer by JAK2/STAT3 axis. *Nature Communications 2018 9:1*, *9*(1), 1–12. https://doi.org/10.1038/s41467-018-05852-8

D, K., M, B., FC, P., MA, M., CV, W., & LC, M. (2012). Ongoing Notch signaling maintains phenotypic fidelity in the adult exocrine pancreas. *Developmental Biology*, *362*(1), 57–64. https://doi.org/10.1016/J.YDBIO.2011.11.010

EL, J., N, W., K, M., RT, B., D, C., R, M., T, J., & DA, T. (2001). Analysis of lung tumor initiation and progression using conditional expression of oncogenic K-ras. *Genes & Development*, *15*(24), 3243–3248. https://doi.org/10.1101/GAD.943001

Golan, T., Atias, D., Stossel, C., & Raitses-Gurevich, M. (2021). Patient-derived xenograft models of BRCA-associated pancreatic cancers. *Advanced Drug Delivery Reviews*, *171*, 257–265. https://doi.org/10.1016/J.ADDR.2021.02.010

Gorgoulis, V. G., Vassiliou, L. V. F., Karakaidos, P., Zacharatos, P., Kotsinas, A., Liloglou, T., Venere, M., DiTullio, R. A., Kastrinakis, N. G., Levy, B., Kletsas, D., Yoneta, A., Herlyn, M., Kittas, C., & Halazonetis, T. D. (2005). Activation of the DNA damage checkpoint and genomic instability in human precancerous lesions. *Nature 2005 434:7035*, *434*(7035), 907–913. https://doi.org/10.1038/nature03485

Gruber, R., Panayiotou, R., Nye, E., Spencer-Dene, B., Stamp, G., & Behrens, A. (2016). YAP1 and TAZ Control Pancreatic Cancer Initiation in Mice by Direct

Up-regulation of JAK–STAT3 Signaling. *Gastroenterology*, *151*(3), 526–539. https://doi.org/10.1053/J.GASTRO.2016.05.006

Halazonetis, T. D., Gorgoulis, V. G., & Bartek, J. (2008). An Oncogene-Induced DNA Damage Model for Cancer Development. *Science*, *319*(5868), 1352–1355. https://doi.org/10.1126/SCIENCE.1140735

Hamarsheh, S., Groß, O., Brummer, T., & Zeiser, R. (2020). Immune modulatory effects of oncogenic KRAS in cancer. *Nature Communications 2020 11:1*, *11*(1), 1–11. https://doi.org/10.1038/s41467-020-19288-6

Hruban, R. H., Goggins, M., Parsons, J., Kern, S. E., G, G. M., & Johns, T. (2000). *Progression Model for Pancreatic Cancer 1*. http://pathology.jhu.edu/pancreas_panin.

J, L., H, G., V, B., I, S.-W., D, H.-B., G, K., W, S., & SA, H. (2001). Allelic loss is often the first hit in the biallelic inactivation of the p53 and DPC4 genes during pancreatic carcinogenesis. *The American Journal of Pathology*, *158*(5), 1677–1683. https://doi.org/10.1016/S0002-9440(10)64123-5

Jemal, A., Siegel, R., Xu, J., & Ward, E. (2010). Cancer Statistics, 2010. *CA: A Cancer Journal for Clinicians*, *60*(5), 277–300. https://doi.org/10.3322/CAAC.20073

Kitajima, S., Thummalapalli, R., & Barbie, D. A. (2016). Inflammation as a Driver and Vulnerability of KRAS Mediated Oncogenesis. *Seminars in Cell & Developmental Biology*, *58*, 127. https://doi.org/10.1016/J.SEMCDB.2016.06.009

Kotsantis, P., Petermann, E., & Boulton, S. J. (2018). Mechanisms of Oncogene-

Induced Replication Stress: Jigsaw Falling into Place. *Cancer Discovery*, *8*(5), 537–555. https://doi.org/10.1158/2159-8290.CD-17-1461

Kuroki, T., Yendamuri, S., Trapasso, F., Matsuyama, A., Aqeilan, R. I., Alder, H., Rattan, S., Cesari, R., Nolli, M. L., Williams, N. N., Mori, M., Kanematsu, T., & Croce, C. M. (2004). The Tumor Suppressor Gene WWOX at FRA16D Is Involved in Pancreatic Carcinogenesis. *Clinical Cancer Research*, *10*(7), 2459–2465. https://doi.org/10.1158/1078-0432.CCR-03-0096

L, M., TA, Z., SM, S., SW, O., HA, Z., H, G., LL, N., RD, P., MJ, H., AR, J., ES, L., & H, Z. (2010). A robust and high-throughput Cre reporting and characterization system for the whole mouse brain. *Nature Neuroscience*, *13*(1), 133–140. https://doi.org/10.1038/NN.2467

Lesina, M., Kurkowski, M. U., Ludes, K., Rose-John, S., Treiber, M., Klöppel, G., Yoshimura, A., Reindl, W., Sipos, B., Akira, S., Schmid, R. M., & Algül, H. (2011). Stat3/Socs3 Activation by IL-6 Transsignaling Promotes Progression of Pancreatic Intraepithelial Neoplasia and Development of Pancreatic Cancer. *Cancer Cell*, *19*(4), 456–469. https://doi.org/10.1016/J.CCR.2011.03.009

Logsdon, C. D., & Ji, B. (2009). Ras Activity in Acinar Cells Links Chronic Pancreatitis and Pancreatic Cancer. *Clinical Gastroenterology and Hepatology : The Official Clinical Practice Journal of the American Gastroenterological Association*, *7*(11 Suppl), S40. https://doi.org/10.1016/J.CGH.2009.07.040

MACGREGOR-DAS, A. M., & IACOBUZIO-DONAHUE, C. A. (2013). Molecular Pathways in Pancreatic Carcinogenesis. *Journal of Surgical Oncology*, *107*(1), 8. https://doi.org/10.1002/JSO.23213

Moskaluk, C. A., Hruban, R. H., & Kern, S. E. (1997). p16 and K-ras Gene Mutations in the Intraductal Precursors of Human Pancreatic Adenocarcinoma. *Cancer Research*, *57*(11).

MP, di M., & CD, L. (2013). Roles for KRAS in pancreatic tumor development and progression. *Gastroenterology*, *144*(6), 1220–1229. https://doi.org/10.1053/J.GASTRO.2013.01.071

MS, S., B, B., J, L., T, D., B, F., JH, C., K, A., H, H., NA, H., F, X., JD, P., CM, A., & K, H. (2017). Wwox-Brca1 interaction: role in DNA repair pathway choice. *Oncogene*, *36*(16), 2215–2227. https://doi.org/10.1038/ONC.2016.389

Nakayama, S., Semba, S., Maeda, N., Aqeilan, R. I., Huebner, K., & Yokozaki, H. (2008). Role of the WWOX gene, encompassing fragile region FRA16D, in suppression of pancreatic carcinoma cells. *Cancer Science*, *99*(7), 1370–1376. https://doi.org/10.1111/J.1349-7006.2008.00841.X

Oncology, R. H. H.]. (2002). Loss of Expression of Dpc4 in Pancreatic Intraepithelial Neoplasia: Evidence That DPC4 Inactivation Occurs Late in Neoplastic Progression 1. *CANCER RESEARCH*, *60*. http://pathology.jhu.edu/pancreas_panin

Perkhofer, L., Schmitt, A., Romero Carrasco, M. C., Ihle, M., Hampp, S., Ruess, D. A., Hessmann, E., Russell, R., Lechel, A., Azoitei, N., Lin, Q., Liebau, S., Hohwieler, M., Bohnenberger, H., Lesina, M., Algül, H., Gieldon, L., Schröck, E., Gaedcke, J., … Kleger, A. (2017). ATM Deficiency Generating Genomic Instability Sensitizes Pancreatic Ductal Adenocarcinoma Cells to Therapy-Induced DNA Damage. *Cancer Research*, *77*(20), 5576–5590.

https://doi.org/10.1158/0008-5472.CAN-17-0634

R, B., CH, M., D, P., G, W., S, R., J, D., J, B., JS, B., J, D., M, U., KT, M. H., RM, P., AH, L., YJ, C., L, H., H, G., M, R., W, W., MS, L., … M, M. (2010). The landscape of somatic copy-number alteration across human cancers. *Nature*, *463*(7283), 899–905. https://doi.org/10.1038/NATURE08822

RI, A., M, A.-R., & M, A.-O. (2014). The common fragile site FRA16D gene product WWOX: roles in tumor suppression and genomic stability. *Cellular and Molecular Life Sciences : CMLS*, *71*(23), 4589–4599. https://doi.org/10.1007/S00018-014-1724-Y

Ryan, D. P., Hong, T. S., & Bardeesy, N. (2014). Pancreatic Adenocarcinoma. *Http://Dx.Doi.Org/10.1056/NEJMra1404198*, *371*(11), 1039–1049. https://doi.org/10.1056/NEJMRA1404198

S, L., & X, W. (2020). Common fragile sites: protection and repair. *Cell & Bioscience*, *10*(1). https://doi.org/10.1186/S13578-020-00392-5

S, N., S, S., N, M., RI, A., K, H., & H, Y. (2008). Role of the WWOX gene, encompassing fragile region FRA16D, in suppression of pancreatic carcinoma cells. *Cancer Science*, *99*(7), 1370–1376. https://doi.org/10.1111/J.1349-7006.2008.00841.X

Schirmer, M. A., Lüske, C. M., Roppel, S., Schaudinn, A., Zimmer, C., Pflüger, R., Haubrock, M., Rapp, J., Güngör, C., Bockhorn, M., Hackert, T., Hank, T., Strobel, O., Werner, J., Izbicki, J. R., Johnsen, S. A., Gaedcke, J., Brockmöller, J., & Ghadimi, B. M. (2016). Relevance of Sp Binding Site Polymorphism in WWOX for Treatment Outcome in Pancreatic Cancer. *JNCI Journal of the*

National Cancer Institute, *108*(5), 387. https://doi.org/10.1093/JNCI/DJV387

Schlesinger, Y., Yosefov-Levi, O., Kolodkin-Gal, D., Granit, R. Z., Peters, L., Kalifa, R., Xia, L., Nasereddin, A., Shiff, I., Amran, O., Nevo, Y., Elgavish, S., Atlan, K., Zamir, G., & Parnas, O. (2020). Single-cell transcriptomes of pancreatic preinvasive lesions and cancer reveal acinar metaplastic cells' heterogeneity. *Nature Communications 2020 11:1*, *11*(1), 1–18. https://doi.org/10.1038/s41467-020-18207-z

Schrock, M. S., Batar, B., Lee, J., Druck, T., Ferguson, B., Cho, J. H., Akakpo, K., Hagrass, H., Heerema, N. A., Xia, F., Parvin, J. D., Aldaz, C. M., & Huebner, K. (2017). Wwox–Brca1 interaction: role in DNA repair pathway choice. *Oncogene*, *36*(16), 2215. https://doi.org/10.1038/ONC.2016.389

Siegel, R. L., Miller, K. D., & Jemal, A. (2015). Cancer statistics, 2015. *CA: A Cancer Journal for Clinicians*, *65*(1), 5–29. https://doi.org/10.3322/CAAC.21254

Siegel, R. L., Miller, K. D., & Jemal, A. (2019). Cancer statistics, 2019. *CA: A Cancer Journal for Clinicians*, *69*(1), 7–34. https://doi.org/10.3322/CAAC.21551

Sikka, S., Surana, R., Dai, X., Zhang, J., Kumar, A. P., Tan, B. K. H., Sethi, G., & Bishayee, A. (2014). Targeting the STAT3 signaling pathway in cancer: Role of synthetic and natural inhibitors. *Biochimica et Biophysica Acta (BBA) - Reviews on Cancer*, *1845*(2), 136–154. https://doi.org/10.1016/J.BBCAN.2013.12.005

SK, A., S, D. M., S, H., M, A.-R., Z, S., J, H., M, R., XA, P., S, R., JL, S., GS, S., JB, L., & RI, A. (2013). Conditional inactivation of the mouse Wwox tumor suppressor gene recapitulates the null phenotype. *Journal of Cellular Physiology*, *228*(7), 1377–1382. https://doi.org/10.1002/JCP.24308

Tanna, M., & Aqeilan, R. I. (2018). Modeling WWOX loss of function in vivo: What have we learned? *Frontiers in Oncology*, *8*(OCT), 420. https://doi.org/10.3389/FONC.2018.00420/BIBTEX

Waddell, N., Pajic, M., Patch, A.-M., Chang, D. K., Kassahn, K. S., Bailey, P., Johns, A. L., Miller, D., Nones, K., Quek, K., Quinn, M. C. J., Robertson, A. J., Fadlullah, M. Z. H., Bruxner, T. J. C., Christ, A. N., Harliwong, I., Idrisoglu, S., Manning, S., Nourse, C., … Grimmond, S. M. (2015). Whole genomes redefine the mutational landscape of pancreatic cancer. *Nature 2015 518:7540*, *518*(7540), 495–501. https://doi.org/10.1038/nature14169

Wang, L., Xie, D., & Wei, D. (2019). Pancreatic Acinar-to-Ductal Metaplasia and Pancreatic Cancer. *Methods in Molecular Biology*, *1882*, 299–308. https://doi.org/10.1007/978-1-4939-8879-2_26

Wilentz, R. E., Geradts, J., Maynard, R., Offerhaus, G. J. A., Kang, M., Goggins, M., Yeo, C. J., Kern, S. E., & Hruban, R. H. (1998). Inactivation of the p16 (INK4A) Tumor-suppressor Gene in Pancreatic Duct Lesions: Loss of Intranuclear Expression. *Cancer Research*, *58*(20).

Yu, H., Pardoll, D., & Jove, R. (2009). STATs in cancer inflammation and immunity: a leading role for STAT3. *Nature Reviews Cancer 2009 9:11*, *9*(11), 798–809. https://doi.org/10.1038/nrc2734

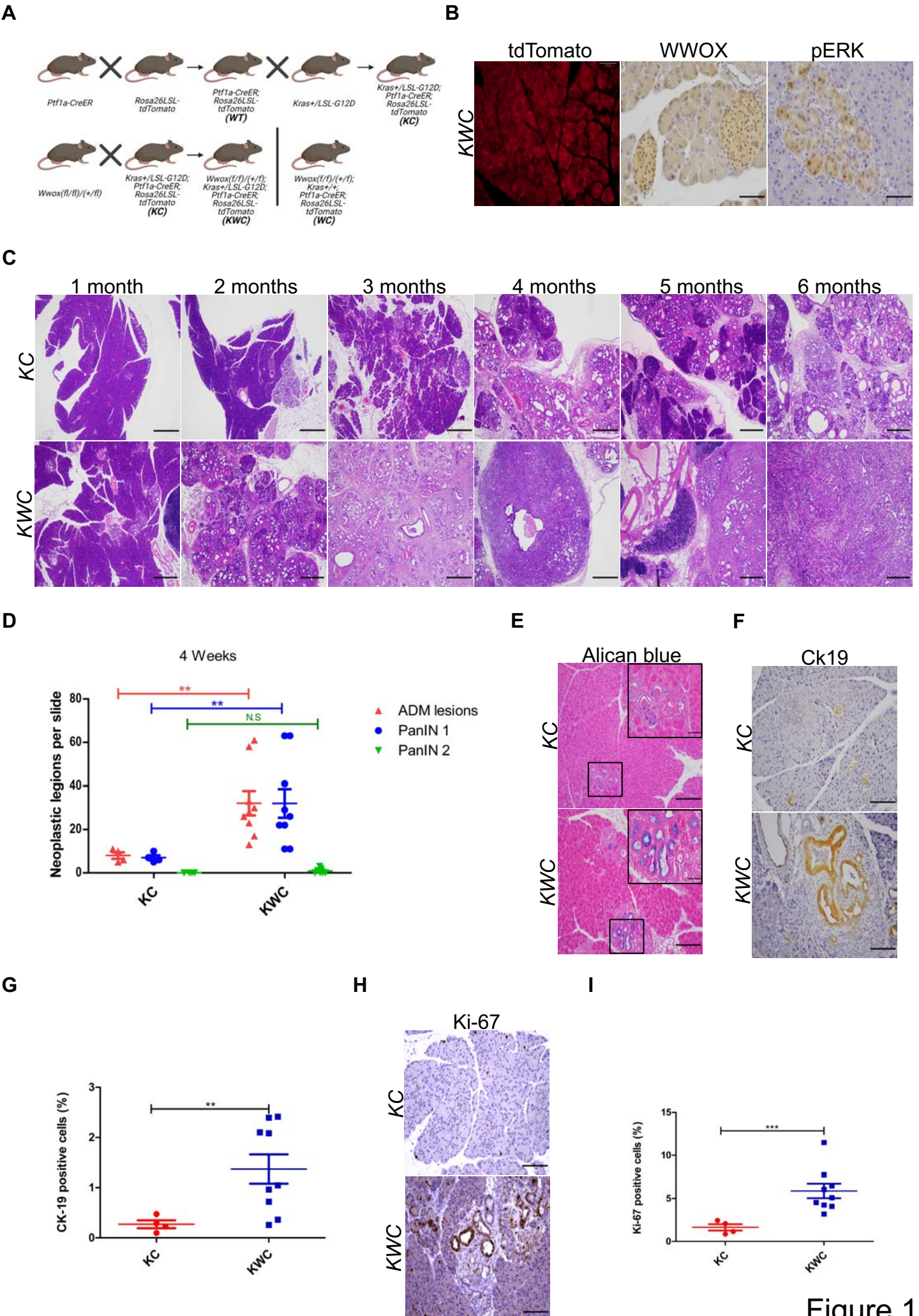
A
Ptf1a-CreER
Rosa26LSL-tdTomato
Ptf1a-CreER; Rosa26LSL-tdTomato (WT)
Kras+/LSL-G12D
Kras+/LSL-G12D; Ptf1a-CreER; Rosa26LSL-tdTomato (KC)
Wwox(fl/fl)/(+/fl)
Kras+/LSL-G12D; Ptf1a-CreER; Rosa26LSL-tdTomato (KC)
Wwox(f/f)/(+/f); Kras+/LSL-G12D; Ptf1a-CreER; Rosa26LSL-tdTomato (KWC)
Wwox(f/f)/(+/f); Kras+/+; Ptf1a-CreER; Rosa26LSL-tdTomato (WC)
B
tdTomato
WWOX
pERK
KWC
C
1 month
2 months
3 months
4 months
5 months
6 months
KC
KWC
D
4 Weeks
Neoplastic legions per slide
80
60
40
20
0
**
**
N.S
KC
KWC
ADM lesions
PanIN 1
PanIN 2
E
Alican blue
KC
KWC
F
Ck19
KC
KWC
G
CK-19 positive cells (%)
3
2
1
0
**
KC
KWC
H
Ki-67
KC
KWC
I
Ki-67 positive cells (%)
15
10
5
0
***
KC
KWC

Figure 1

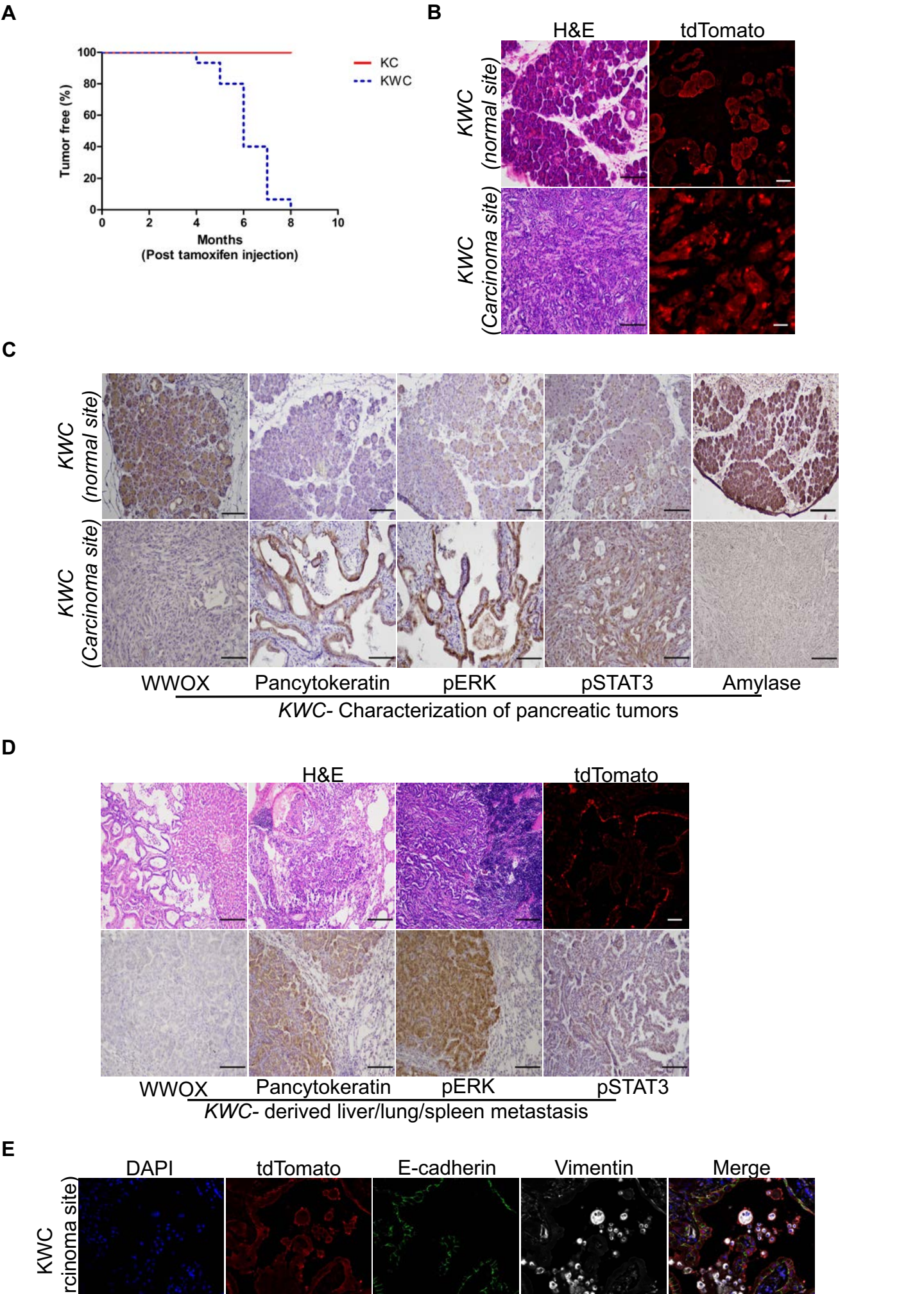
A
Tumor free (%)
100
80
60
40
20
0
0
2
4
6
8
10
Months
(Post tamoxifen injection)
KC
KWC
B
H&E
tdTomato
KWC (normal site)
KWC (Carcinoma site)
C
KWC (normal site)
KWC (Carcinoma site)
WWOX
Pancytokeratin
pERK
pSTAT3
Amylase
KWC- Characterization of pancreatic tumors
D
H&E
tdTomato
WWOX
Pancytokeratin
pERK
pSTAT3
KWC- derived liver/lung/spleen metastasis
E
DAPI
tdTomato
E-cadherin
Vimentin
Merge
KWC (Carcinoma site)

Figure2

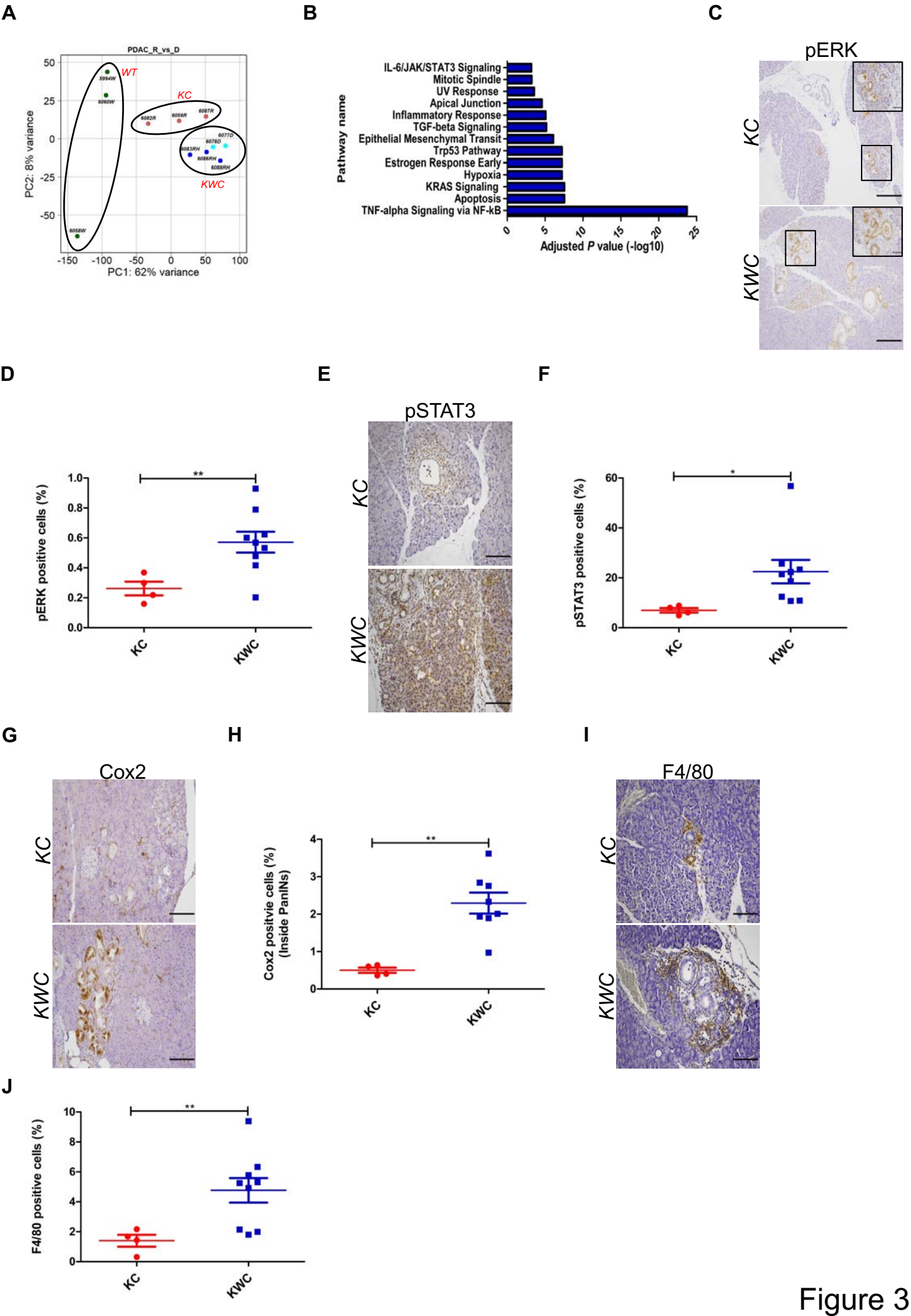
A
PDAC_R_vs_D
WT
KC
KWC
PC2: 8% variance
PC1: 62% variance
B
Pathway name
IL-6/JAK/STAT3 Signaling
Mitotic Spindle
UV Response
Apical Junction
Inflammatory Response
TGF-beta Signaling
Epithelial Mesenchymal Transit
Trp53 Pathway
Estrogen Response Early
Hypoxia
KRAS Signaling
Apoptosis
TNF-alpha Signaling via NF-kB
Adjusted P value (-log10)
C
pERK
KC
KWC
D
pERK positive cells (%)
KC
KWC
E
pSTAT3
KC
KWC
F
pSTAT3 positive cells (%)
KC
KWC
G
Cox2
KC
KWC
H
Cox2 positvie cells (%) (Inside PanINs)
KC
KWC
I
F4/80
KC
KWC
J
F4/80 positive cells (%)
KC
KWC

Figure 3

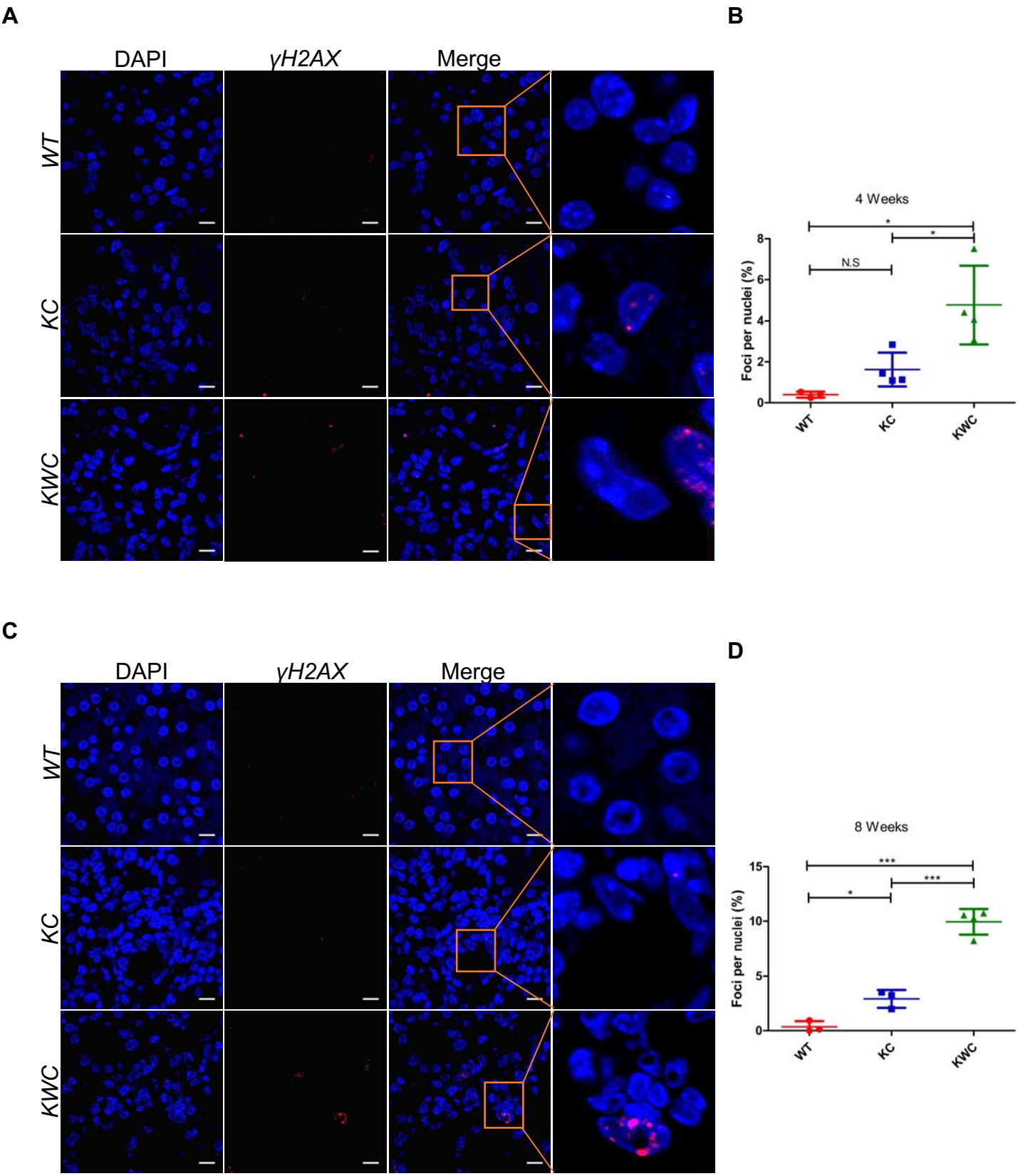
A
DAPI
γH2AX
Merge
WT
KC
KWC
B
4 Weeks
Foci per nuclei (%)
N.S
*
*
WT
KC
KWC
C
DAPI
γH2AX
Merge
WT
KC
KWC
D
8 Weeks
Foci per nuclei (%)
***
***
*
WT
KC
KWC

Figure 4

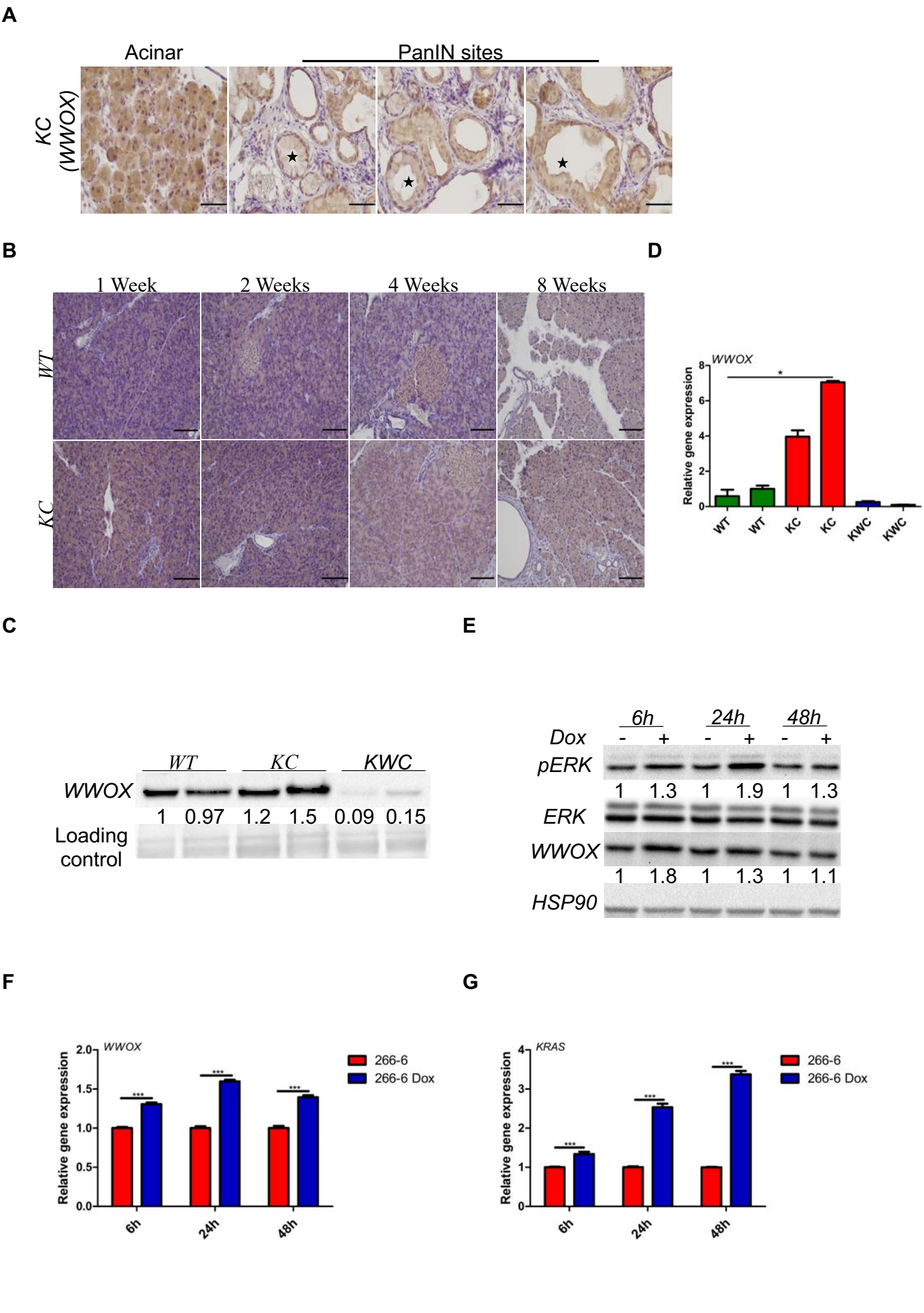
A
Acinar
PanIN sites
KC (WWOX)
B
1 Week
2 Weeks
4 Weeks
8 Weeks
WT
KC
D
WWOX
Relative gene expression
WT
WT
KC
KC
KWC
KWC
C
WT
KC
KWC
WWOX
1 0.97 1.2 1.5 0.09 0.15
Loading control
E
6h
24h
48h
Dox
- + - + - +
pERK
1 1.3 1 1.9 1 1.3
ERK
WWOX
1 1.8 1 1.3 1 1.1
HSP90
F
WWOX
Relative gene expression
266-6
266-6 Dox
6h
24h
48h
G
KRAS
Relative gene expression
266-6
266-6 Dox
6h
24h
48h

Figure 5

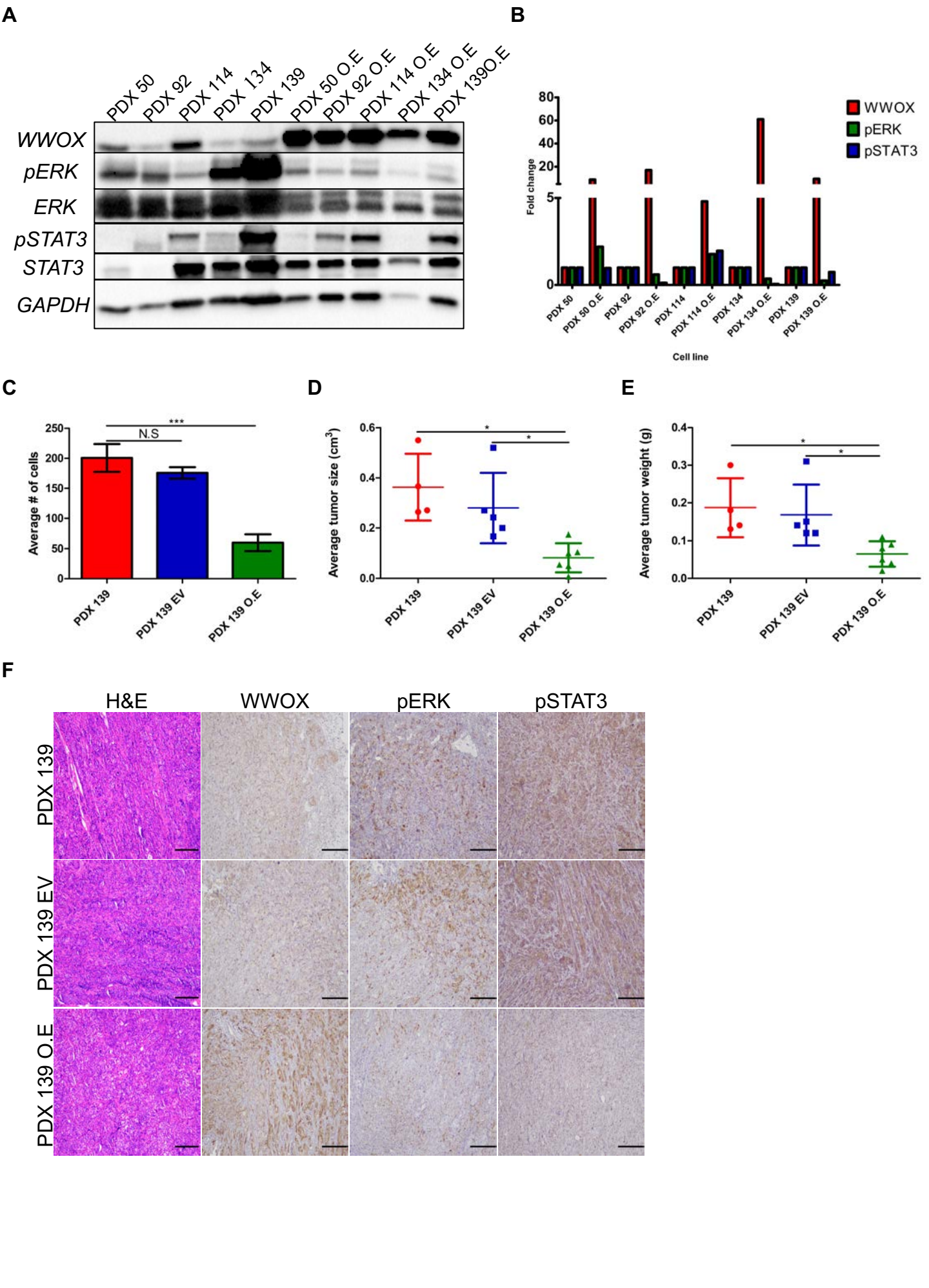
A
PDX 50
PDX 92
PDX 114
PDX 134
PDX 139
PDX 50 O.E
PDX 92 O.E
PDX 114 O.E
PDX 134 O.E
PDX 139O.E
WWOX
pERK
ERK
pSTAT3
STAT3
GAPDH
B
WWOX
pERK
pSTAT3
Fold change
Cell line
C
Average # of cells
N.S
***
PDX 139
PDX 139 EV
PDX 139 O.E
D
Average tumor size (cm3)
E
Average tumor weight (g)
F
H&E
WWOX
pERK
pSTAT3
PDX 139
PDX 139 EV
PDX 139 O.E

Figure 6

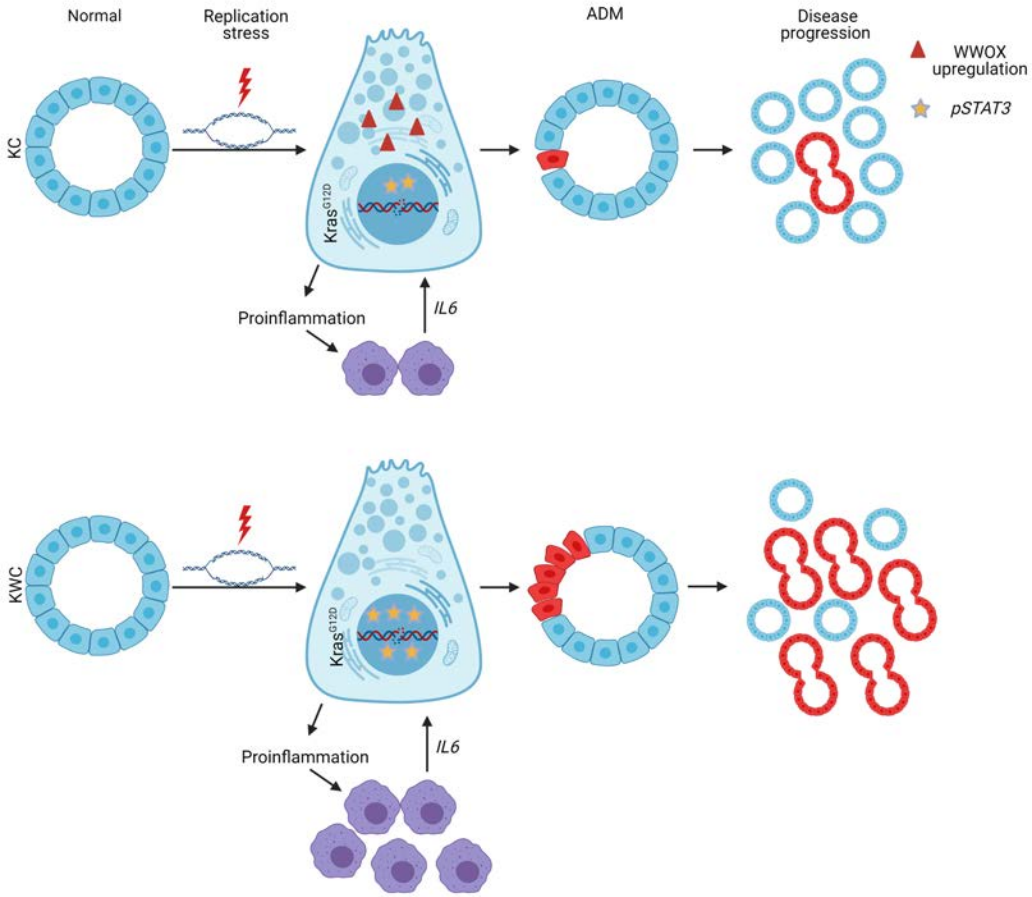
Normal
Replication stress
ADM
Disease progression
WWOX upregulation
pSTAT3
KC
KrasG12D
Proinflammation
IL6
KWC
KrasG12D
Proinflammation
IL6

Figure 7

Supplementary Figure Legends:

Supplemental Figure 1. Validation of mice model. (A) Genotyping PCR for DNA extracted from mice tails showing expression of Cre recombinase with its negative control, WWOX wild type and floxed alleles, $Kras^{G12D}$ and wild type alleles respectively. (B) Bright field imaging of tomato expression in total pancreas attached to spleen. (C) Western blot of WWOX in KWC mice compared to KC mice. (D) Upper panel- H&E stain of WC mice 11 months post tamoxifen injection (magnification, ×10). Lower panel- pERK stain of WC mice 11 months post tamoxifen injection (magnification, ×10). (G) WWOX stain performed in parallel for all the sections: WT, WC, KC, KWC (Hetro), and KWC (Homo) respectively (magnification, ×20). (E) Tomato and amylase stain in acinar cells (magnification, ×40). (F) RNAseq data of ADM genes (Runx1, Onecut2, and Foxq1 respectively) in WT, KC, KWC mice respectively. *P<0.05. Two tail unpaired t test. Quantification graphs represent the means ± SD.

Supplemental Figure 2. Characterization of KWC normal sites. (A) Representative H&E (magnification ×10), WWOX, pancytokeratin, pERK, and pStat3 stain for normal KWC site (magnification, ×10). (B) Upper panel- representative tomato stain for WT pancreas mice (magnification ×40). Middle panel- representative tomato stain for WT liver mice (Scale bar ×40). Lower panel- representative tomato stain for WT lung mice (magnification ×40). (C) Representative tomato, E-cadherin, and vimentin stain of KWC PanINs site (magnification ×40).

Supplemental Figure 3. Activation of inflammatory effector genes upon WWOX activation. (A) Relative gene expression of Socs3 from RNAseq data. (B) RT-PCR of IL6 for acinar cells, 4 weeks post tamoxifen injection for WT mice (n=2), KC mice (n=3), and KWC mice (n=3). (C) Relative gene expression of Il6 from RNAseq data. (D) Relative gene expression of Cox2 from RNAseq data. NS>0.05, **P*<0.05, ***P*<0.001. Two tail unpaired t test. Quantification graphs represent the means ± SD.

Supplemental Figure 4. Accumulation of 53BP1 complex upon deletion of WWOX. (A) Representative 53bp1 stain at ADM site of WT (n=3), KC (n=3), and KWC mice (n=4) respectively, 4 weeks post tamoxifen injection (magnification ×60). (B) Quantification of 53bp1stain in A. (C) Representative 53BP1 stain at ADM site of WT (n=3), KC (n=3), and KWC mice (n=3) respectively, 8 weeks post tamoxifen injection (magnification ×60). (D) Quantification of 53BP1 stain in C. **P*<0.05, ***P*<0.001, ****P*<0. 0001, by two tail unpaired t test. Quantification graphs represent the means ± SD.

Supplemental Figure 6. WWOX restoration to PDXs with already high WWOX expression has no effect on cell aggressiveness. (A) Representative bright field imaging of colony formation for PDX 139, PDX 139 EV, and PDX 139 WWOX O.E (Scale bar 2mm). (B) Representative γH2AX stain for PDX 139, PDX 139 EV, and PDX 139 WWOX O.E. (magnification ×60). (C) Quantification of γH2AX stain in Fig (F). (D) Colony formation of PDX 50, 114, 92, and 134 respectively. NS>0.05, **P*<0.05, ***P*<0.001, ****P*<0. 0001, by two tail unpaired t test. Quantification graphs represent the means ± SD.

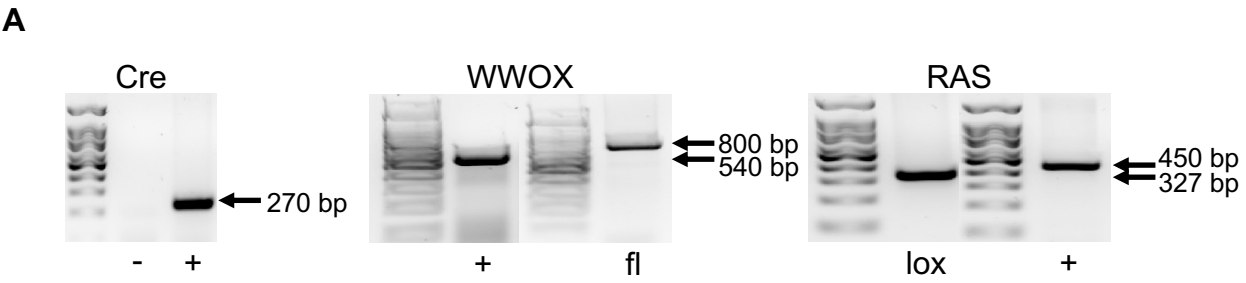
A
Cre
270 bp
- +
WWOX
800 bp
540 bp
+ fl
RAS
450 bp
327 bp
lox +

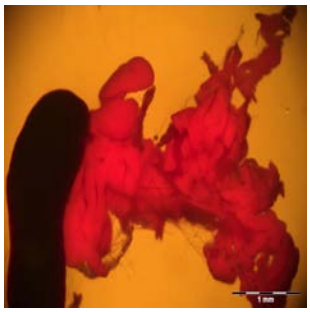
B

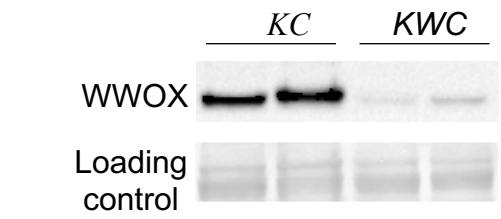
C
KC
KWC
WWOX
Loading control

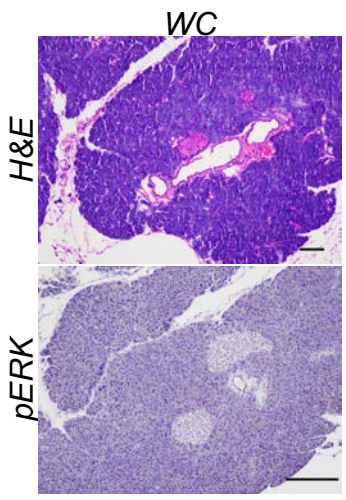
D
WC
H&E
pERK

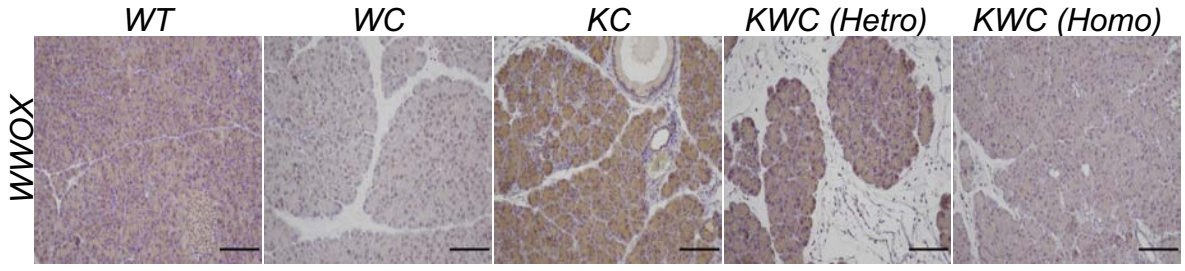
G
WT
WC
KC
KWC (Hetro)
KWC (Homo)
WWOX

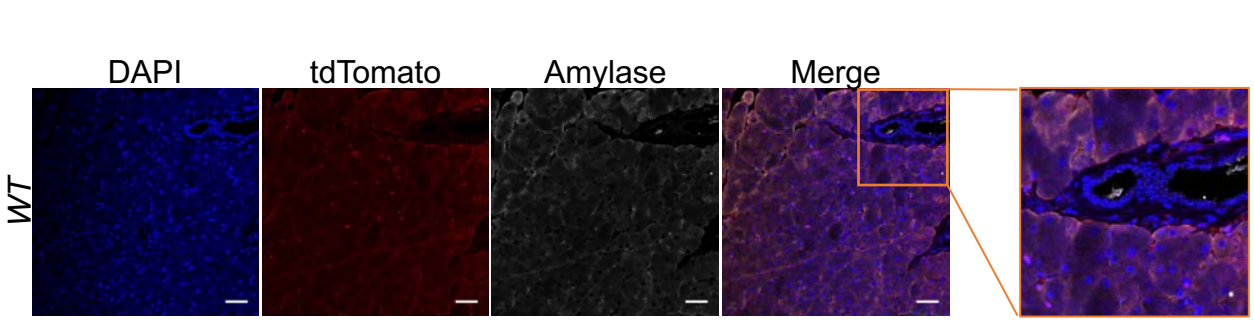
E
DAPI
tdTomato
Amylase
Merge
WT

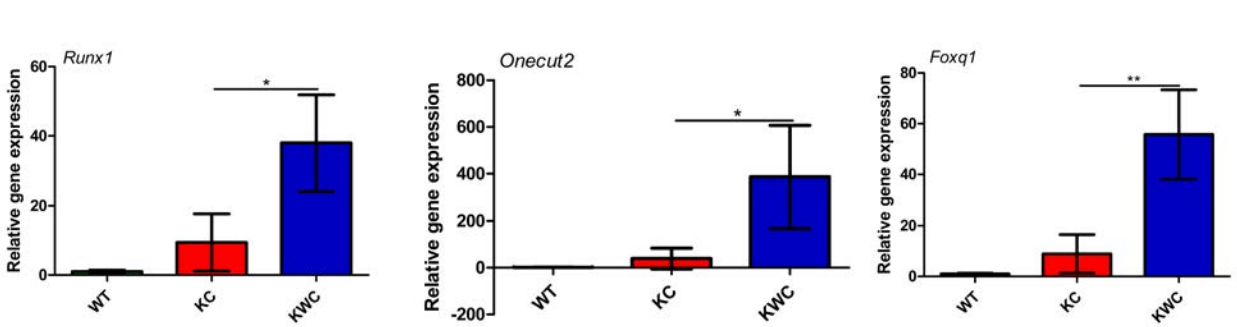
F
Runx1
Relative gene expression
WT
KC
KWC
Onecut2
Foxq1

Figure S1

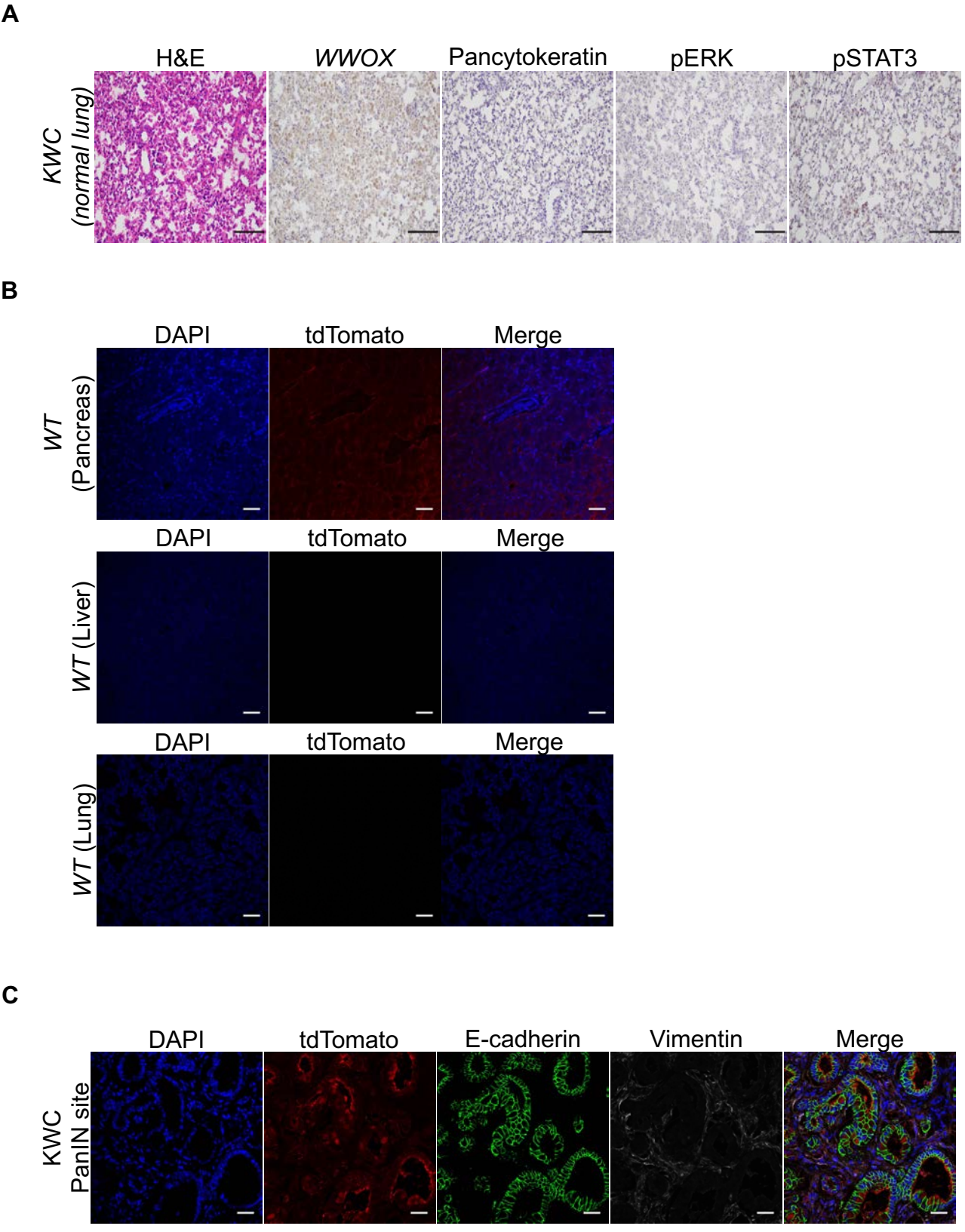
A
H&E
WWOX
Pancytokeratin
pERK
pSTAT3
KWC (normal lung)
B
DAPI
tdTomato
Merge
WT (Pancreas)
DAPI
tdTomato
Merge
WT (Liver)
DAPI
tdTomato
Merge
WT (Lung)
C
DAPI
tdTomato
E-cadherin
Vimentin
Merge
KWC PanIN site

Figure S2

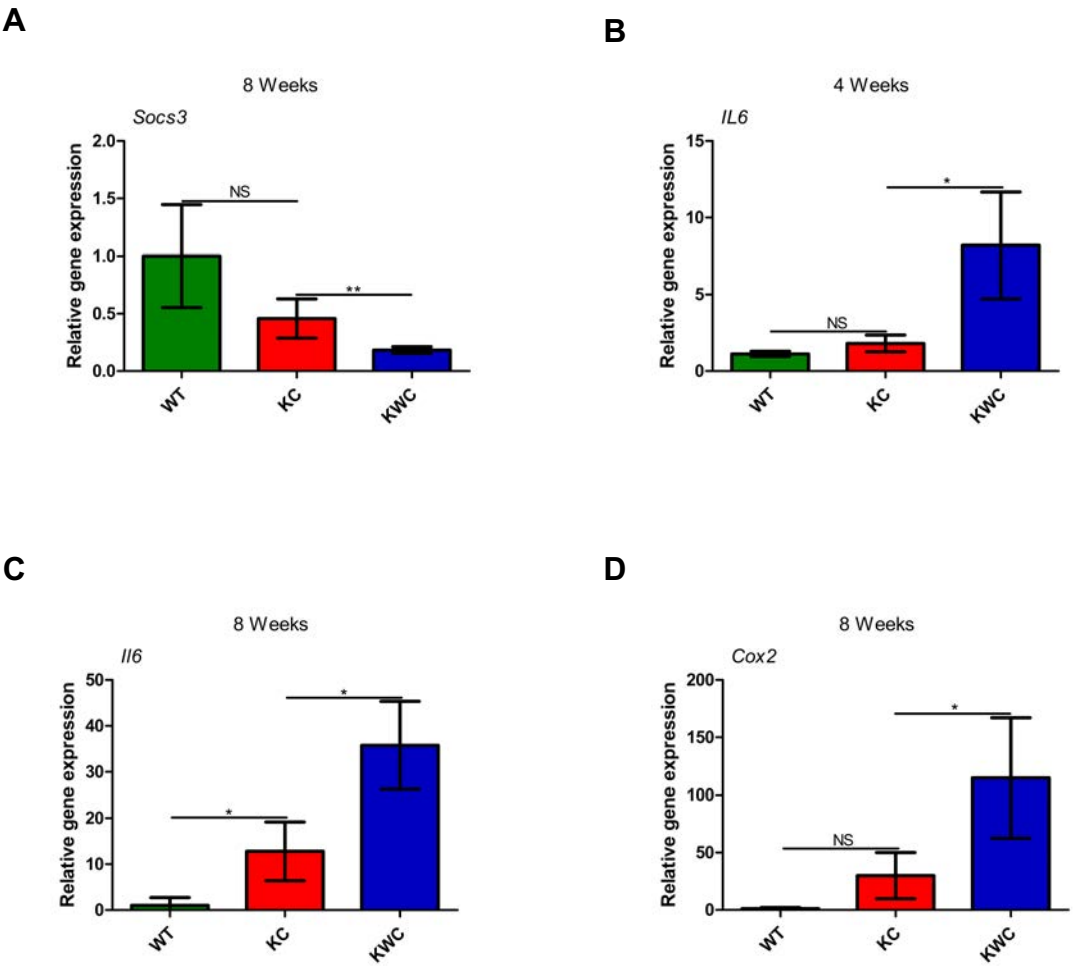
A
8 Weeks
Socs3
Relative gene expression
2.0
1.5
1.0
0.5
0.0
NS
**
WT
KC
KWC
B
4 Weeks
IL6
Relative gene expression
15
10
5
0
*
NS
WT
KC
KWC
C
8 Weeks
Il6
Relative gene expression
50
40
30
20
10
0
*
*
WT
KC
KWC
D
8 Weeks
Cox2
Relative gene expression
200
150
100
50
0
*
NS
WT
KC
KWC

Figure S3

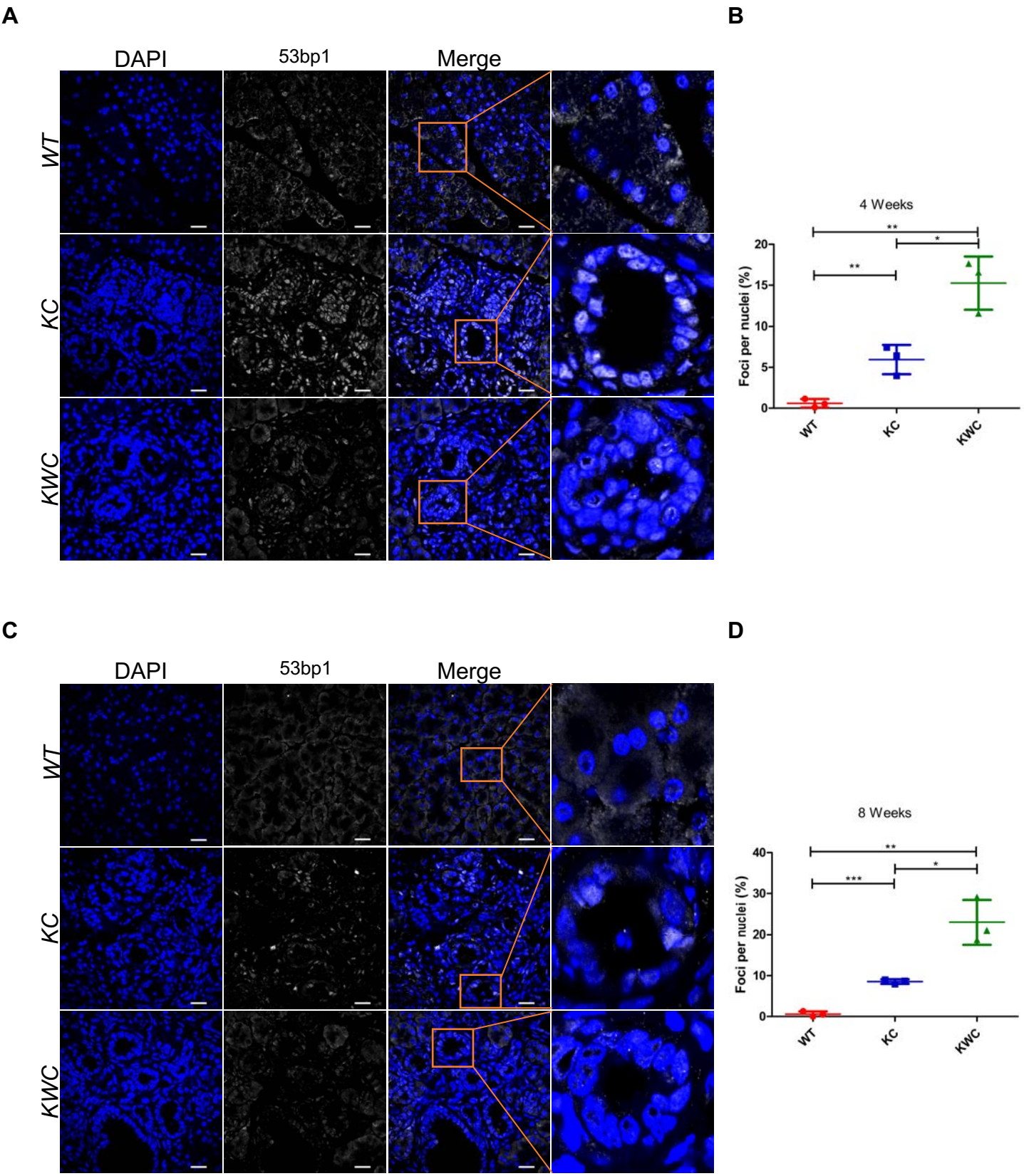
A
DAPI
53bp1
Merge
WT
KC
KWC
B
4 Weeks
Foci per nuclei (%)
20
15
10
5
0
**
*
**
WT
KC
KWC
C
DAPI
53bp1
Merge
WT
KC
KWC
D
8 Weeks
Foci per nuclei (%)
40
30
20
10
0
**
*
***
WT
KC
KWC

Figure S4

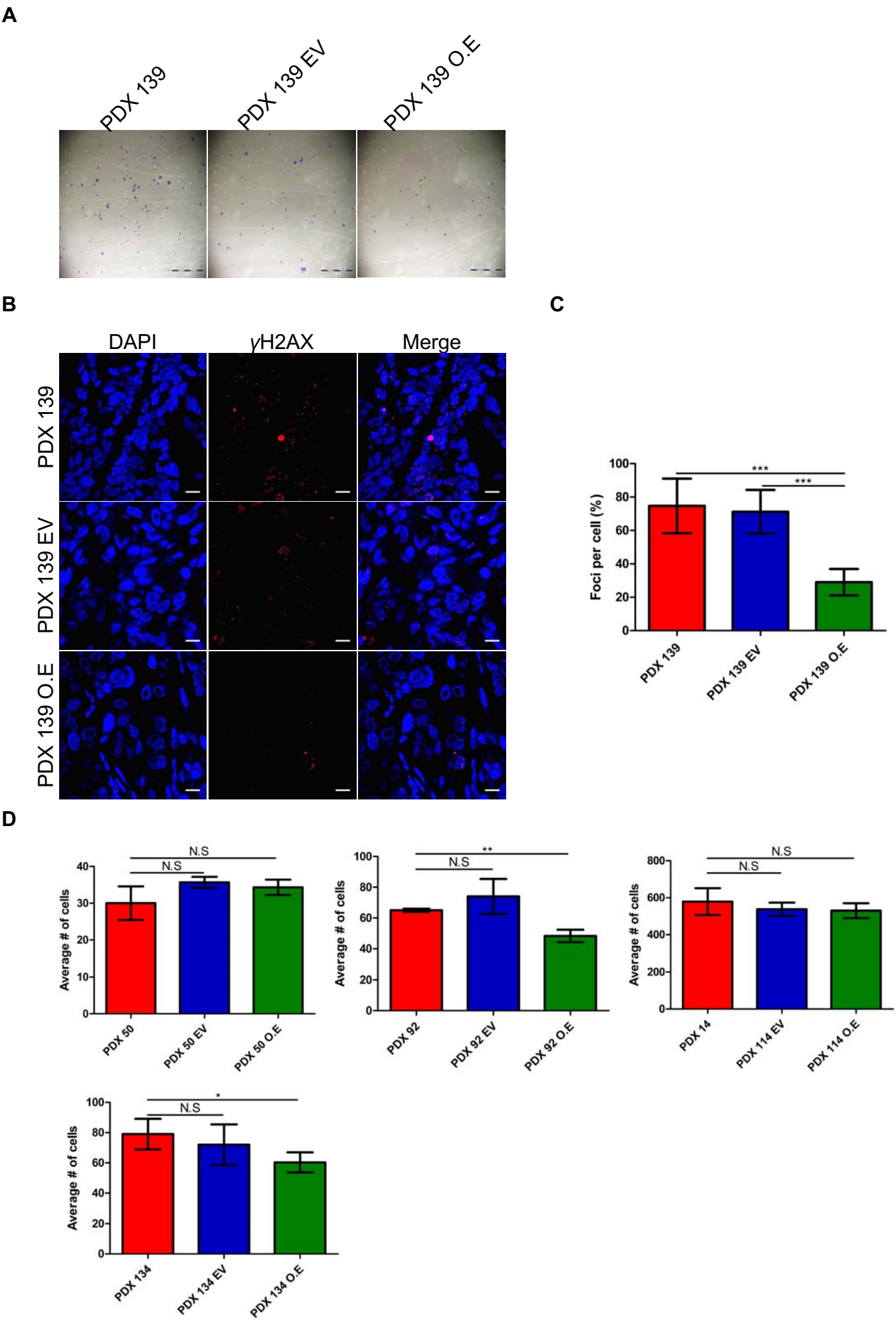
A
PDX 139
PDX 139 EV
PDX 139 O.E
B
DAPI
γH2AX
Merge
PDX 139
PDX 139 EV
PDX 139 O.E
C
Foci per cell (%)
***
***
PDX 139
PDX 139 EV
PDX 139 O.E
D
Average # of cells
N.S
N.S
PDX 50
PDX 50 EV
PDX 50 O.E
**
N.S
PDX 92
PDX 92 EV
PDX 92 O.E
N.S
N.S
PDX 14
PDX 114 EV
PDX 114 O.E
*
N.S
PDX 134
PDX 134 EV
PDX 134 O.E

Figure S5